Subinertial Finestructure on the Continental Slope/Rise Transition

KURT L. POLZIN
Woods Hole Oceanographic Institution

(Preprint, not for general distribution.)

ABSTRACT

Subinertial flucuations having periods of 1-2 days, vertical wavelengths of 250-400 m, horizontal wavelengths of 10-15 km, and peak-to-peak amplitudes of 0.1 m s^{-1} are observed at the base of the continental slope just north of Cape Hatteras. Evidence is presented to suggest that these fluctuations represent the by-product of an instability of the larger scale and lower frequency flow. The momentum, energy and potential vorticity balances of this system are addressed.

1. Introduction

A companion paper (Polzin et al., in preparation) describes the spatial variability of fine- and microstructure in a section across the continental slope and Gulf Stream just north and downstream of Cape Hatteras. Turbulent dissipation is enhanced at the boundary and weak in the interior, despite the fact that the Gulf Stream is much more energetic than flows on the continental slope. Turbulent dissipation is a maximum at the continental slope/rise transition (Figure 1), at about 1200 m water depth.

Data from a Moored Profiler (MP, Doherty et al. 1999) array deployed at the continental slope/rise transition, demonstrates that temporal variability in turbulent dissipation coincides with the presence of finestructure having an intrinsic frequency $\omega = \sigma - k\overline{u} < f$, in which σ is the Eulerian frequency, the product between horizontal wavenumber (k) and background velocity ($\overline{u}$) represents the Doppler shift and f is the Coriolis frequency. That is, the finestructure is not consistant with freely propagating internal waves having $\omega > f$.

The forcing of subinertial motions by the diurnal tide has previously been invoked to explain enhanced fine- and microstructure atop isolated seamounts (Kunze-Toole, Codiga and Eriksen & Brink-Chapman). Topographic waves trapped to the seamount by the finite extent of the topographic waveguide have been invoked to explained such observations (Codiga and Eriksen & Brink-Chapman), though a vortex trapped near-inertial internal wave (Kunze and Toole) appears to best explain the observations in at least one case. The finestructure observed here is not consistent with extant descriptions of topographic edge waves (Rhines 1970).

The fine- and microstructure data presented here are interpreted as being associated with subinertial ($\omega < f$) internal waves resulting from an instability process.

2. Subinertial Finestructure

The $TWIST$ (Turbulence and Waves above Irregular, Sloping Topography) experiment was conceived under the hypothesis that the fine scale wavefield above topographic roughness would have the horizontal scale of that roughness superimposed upon it. Roughness in the form of ridges and gulleys running approximately onshore/off-shore is common on the continental slope and rise in the Mid-Atlantic Bight. The roughness complicates issues of internal wave generation and scattering by introducing smaller scales than typical of rise/slope/shelf topology. A site just north of Cape Hatteras was selected based upon the approximate uniformity of amplitude and roughness scale in the along-slope direction. Horizontal wavelengths of 2.5-3 km and amplitudes of less than 50 m characterize the upper slope (water depths less than 500 m, Figure 2), while dominant wavelengths of about 30 km and amplitudes in excess of 100 m characterize the continental rise at about 2000 m water depth.

A field program was conducted from May 10 - June 8, 1998. This field program, described in greater detail in a companion paper (Polzin et al., in preparation), utilized a variety of vertically profiling instrumentation including the freely falling High Resolution Profiler (Schmitt et al. 1988) which obtains samples of the ocean's temperature, salinity, and horizontal velocity field as well as associated dissipation rates of turbulent kinetic energy and temperature variance. There are three significant limitations to these HRP data. First, there are two temporal gaps associated with the loss of the instru-

Corresponding author address: Kurt L. Polzin, MS#21 WHOI Woods Hole MA, 02543
E-mail: kpolzin@whoi.edu

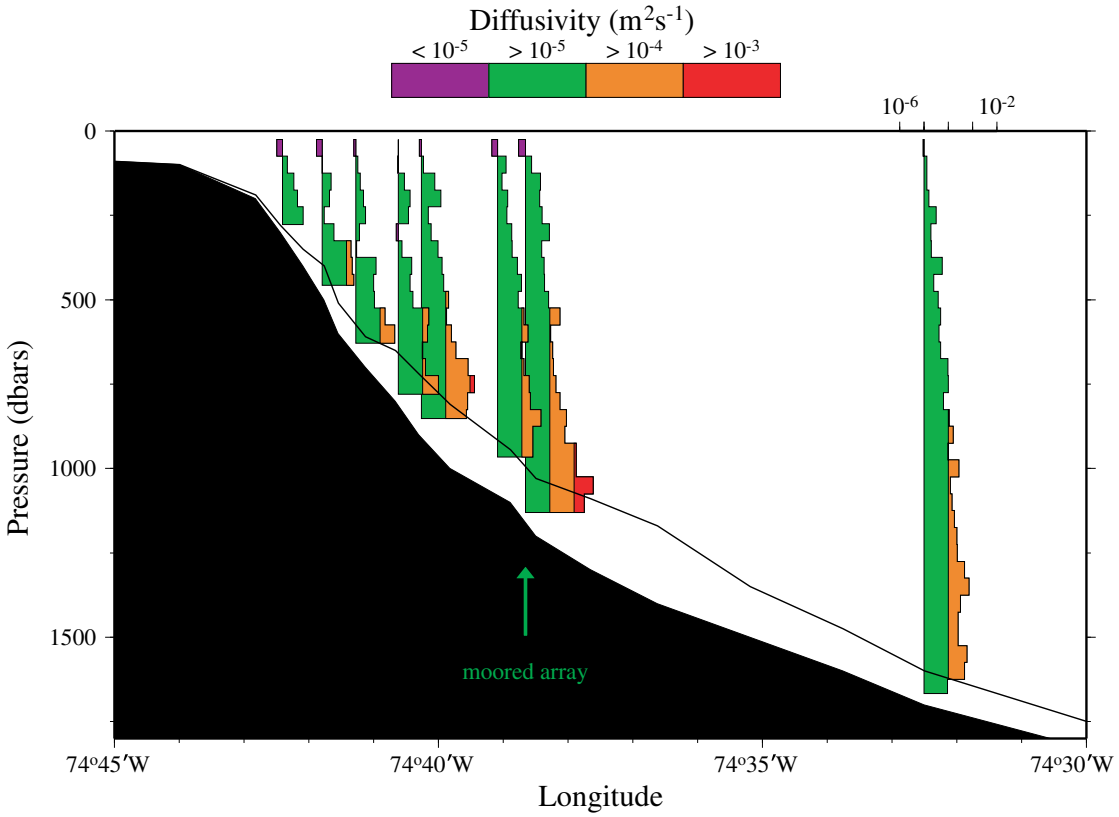

FIG. 1. Averaged profiles of vertical diffusivity ($0.25\epsilon/N^2$) from the reoccupied grids. The diffusivity estimates are plotted on a logarithmic axis with a decadal color scheme. From left to right, the profiles represent the 'C' grid (the first four profiles), the 'L' grid, 'TS1', 'K' and 'N'. Dark shading represents topography within a valley. The solid black line represents the height of adjacent topographic ridges. Individual profiles in the 'L', 'K' and 'N' grids were obtained along isobaths, so that the position of the corresponding average vertical diffusivity profile in longitude corresponds to the western most profile of that grid. The longitude of the eastern most station of a grid can be ascertained by drawing a horizontal line eastward, from the bottom of the vertical profile to beyond the intersection with the solid black line. This figure gives the distinct impression that turbulent mixing is greatest in the vicinity of the moored array. Care needs to be taken with this interpretation, though. The intensity of the turbulent mixing was not constant in time. The fifth, seventh and eigth profiles (from left to right) are representative spatial and temporal averages. In constrast, the first four profiles were obtained at the end of the experiment and the sixth profile was obtained at the beginning. Data from the fifth and seventh profiles, which have better temporal resolution, indicate a maximum in turbulent mixing during the middle portion of the field program. This temporal variability in turbulent mixing can be linked to distinct features in the velocity field. *Use* $\Gamma = 0.20$. *Add isopycnals to figure*

ment. Second, profiles were typically terminated 60-80 above the bottom for most of the experiment. Finally, the instrument uses and acoustic travel time current meter to sense relative velocity and estimates of oceanic velocity are produced by using a dynamical model for the response of the profiler to this relative flow. The dynamical model integrates the relative velocity measurements. Thus, if the offsets (zeros) of the acoustic current meter are not precisely determined, false linear trends are introduced into the estimates of the oceanic velocity profile. These trends were minimized by adjusting the depth mean and linear trend to match those obtained with the ship board acoustic doppler current profiler.

The newly developed Moored Profiler [or MP, (Doherty et al. 1999)], which autonomously samples oceanic finescale velocity, temperature and salinity variability, was also deployed. Three moored profilers were deployed in a closely spaced array, Figure 2. The MPs were set to simultaneously initiate a profile covering 15 m off bottom to approximatly 90 m water depth once every hour-and-a-half. The travel time took about one hour. Thus samples at the top and bottom are separated in time by either one-half-hour or two and one-half-hours. The raw MP data were averaged into 2 m depth bins. Most of the figures below were prepared by first interpolating the 2 m data onto a 20 m by 1.5 hour grid. The time coordinate in this paper uniformly references the deployment of MP 'A' (Figure 2) as the origin.

There are three primary limitations of these MP data. First, despite covering over 90% of the water column, only about 2/3 was covered if depth (z) is streched as $z' = zN_o/N(z)$ using buoyancy frequency $N(z)$ with reference N_o. Our focus here is on the lower half of the water column. Second, the deployments were only of limited duration (16-19 days). Third, the moored array does not resolve the entire slope.

Unless specifically noted, the velocity profile data are analyzed and presented in a coordinate system rotated counter-clockwise by $72.4°$. This rotation approximates the orientation of the 100 m isobath at the shelf break. The rotated coordinate system is referred to as "along-" and "across-" (positive onshore) with the implicit recognition that roughness makes a local definition of the orientation of the continental slope imprecise. A right hand coordinate system $(along, across, up)$ with velocity (u, v, w) and wavenumber $\mathbf{k} = (k, l, m)$, $k_h = (k^2 + l^2)^{1/2}$, is used.

Inspection of the gridded data (Figure 3) suggested the density and velocity fields could be filtered into the following bands delineated by period $\tau = 2\pi/\omega$:

- mean: average over mooring duration
- low: $\tau >$ 4.5 days
- band-passed: 4.5 days $< \tau <$ 18 hours
- tidal: 18 hours $< \tau <$ 7.5 hours

in which the inertial period at 36.5 N is slightly more than 20 hours. Near-inertial motions make little contribution to the variability below about 250 m.

a. low-passed

The low-passed along field is dominated by a two-week period ocscillation having large vertical scale. Maximum velocities exceed -0.25 m s^{-1} at mid-depth (300 m). Upward phase propagation is apparent early in the record and preceeds the velocity maximum. A less robust downward phase propagation is apparent during the second week. In contrast, the isopycnal field exihibits straining between 150-500 m over days 1-5 that is more consistant with a mode-like response. At depth, isopycnals are displaced by over 300 m (1/4 of the entire water column!) during the initial week.

The low-passed across field exhibits higher frequency content and smaller vertical scale than the along field. There is a pronounced downward phase propagation in the latter two-thirds of the record. Downward phase propagation at depths of 200-600 m over days 11-17 is also apparent is the isopycnal field.

The observed phase propagation is strongly suggestive of a wave-like response and the frequencies are sufficiently high as to imply that topographic effects provide the dominant restoring force. Topographic edge waves [Rhines (1970)] exhibit phase propagation in the vertical (see appendix). On the other hand, the observed lack of rectilinear polarization does not agree well with a the single topographic edge wave. Neither are the currents obviously bottom trapped, but one might hypothesize the existence of a drag that alters the typical velocity profile.

The low-passed fields could represent a combination of such waves, as a response to atmospheric forcing. In that case the observed vertical phase propagation could be an artifact of waves having little or no phase variation in the vertical (such as a Kelvin wave) as they disperse from the source. The fields are not documented fully enough to be decomposed into a sum of such waves.

I am strongly inclined towards interpreting the low-passed fields as a response to forcing. Several HRP casts were obtained (one at 475 and one at 625 m water depth) prior to the loss of that instrument and the onset of a Nor'easter. These casts document the transition between shelf (with salinities less than 33 psu) and slope waters (having salinities in excess of 35 psu) lying at about 100 m on day -5. The moored data document this transition at about 150 m on day 0. Upwelling of this transition is seen in the moored data (Fig. 4) as the disappearence of the lightest density classes by day 6. On day one, HRP data at 1300 and 1060 m water depth indicate that the transition had relatively small slopes in the across direction. This depression and presumed across transport of Shelf Water may represent a response to that Nor'easter. Unfortunately, the limited sampling prior to this event limits us from saying anything of greater significance.

b. band-passed

The band-passed fields are dominated by fluctuations of one to two days having relatively small vertical scales, Fig. 5. These fluctuations are also apparent in HRP profiles. All three fields appear to be dominated by upward phase propagation, though instances of downward phase propagation are occasionally present.

Two regimes are apparent in the band-passed fields. The upper part of the water column is dominated by fluctuations in the along-velocity during the first half of the record. Fluctuations of across-velocity dominate the lower portion of the water column during the middle part of the record. These latter features exhibit a nearly monochromatic, wavelike appearence and are the subject of investigation in the rest of the paper.

These high wavenumber band-passed features appear at the time of maximum low-passed along current, Figure 6. They subside as the low-passed along current reverses direction. Slightly higher frequency content is apparent earlier in the record.

Given the nearly monochromatic nature of the fluctuations, dominant wavelengths and periods were estimated from lag coherences of the across velocity in the spatial and temporal domains. Relative minima and maxima of the lag coherence function were interpreted in terms of a plane wave of the form $exp(i[kx + ly + mz - \sigma t])$. This procedure returns a wavenumber-frequency estimate of

- $\mathbf{k} = 2\pi$(-1/15 km, -1/10 km, 1/250 to 1/400 m)

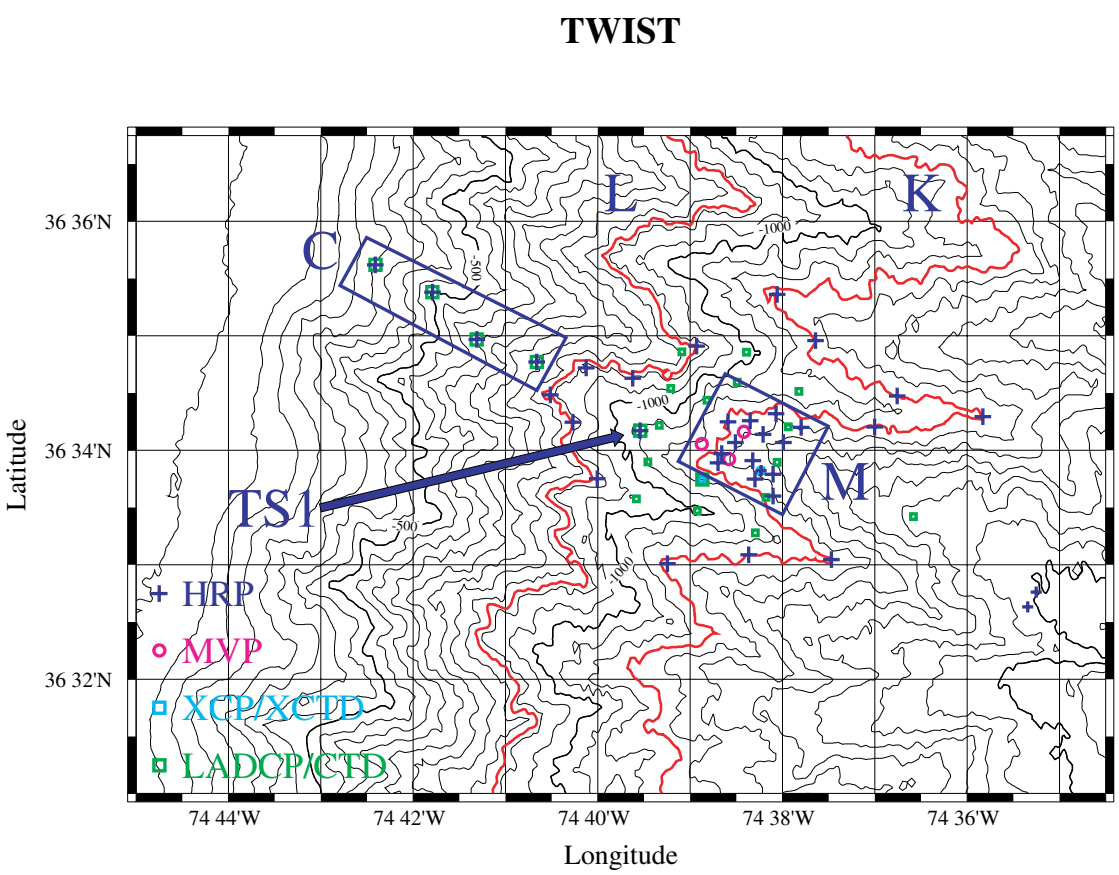

FIG. 2. A partial sampling plan for the TWIST (Turbulence&Waves over Irregularly Sloping Topography) field program. Bathymetry is contoured in intervals of 50 m. The symbol and color key for the various instruments appears within the plots. Large symbols denote re-occuppied stations. The red bathymetric contours denote water depths of 880, 1150 and 1670 m. The HRP work was confined to these bathymetric contours for most of the field program. The 'L', 'K' and 'N' notation signifies grids of reoccupied stations on the 880, 1150 and 1670 m isobaths, respectively. The 'M' notation denotes a repeated grid about the MP array, and 'C' denotes an across shelf grid in waters shallower than 800 m. Time series are depicted with the notation 'TS'. The moored data were obtained within the 'M' grid box with the mooring positions denoted as circles. MP 'A' is to the northeast, 'B' to the southeast and 'C' was deployed along a slightly shallower isobath to the west.

- $\sigma = 2\pi/24$ to $2\pi/45$ hours

for the time period day 4 - day 11 and depth interval 700-1000 m.

Thus the observed features do not have the horizontal scale of the local bathymetry (2.5-3 km wavelength) imprinted upon them [though, notably, the topographic variability in somewhat deeper water (2000 m) on the continental rise exhibits such horizontal scales]. These horizontal wavenumber estimates are also needed to estimate the intrinsic, or non-Doppler shifted, frequency, $\omega = \sigma - k\overline{u}$, where $\overline{u}$ is the low-pass along velocity. The wavenumber estimates returns a sub-inertial intrinsic frequency ($\omega < f$) with negative along (southward) flow. Phase propagation in the across direction is toward shallow water, i.e. westward in the sense of topographic Rossby wave dynamics.

As with the low-passed data, the band-passed observations were compared with topographic edge waves described by Rhines (1970) using parameters for this data set (see the Appendix). In short, this comparison does not return good agreement. Particularly glaring is the discrepancy between observed and predicted vertical structure. Such differences led us to consider a heirarchy of increasingly complicated models: non-uniform topography, diabatic effects, nonlinearity, combinations of waves and modification of the waves by the presence of a mean flow. While not unique, the most plausible explanation is believed to be provided by considering the effects of the presence of the lower frequency flow field.

c. tidal

Along velocities are enhanced in the later part of the record and greater vertical coherence of the isopycnal dis-

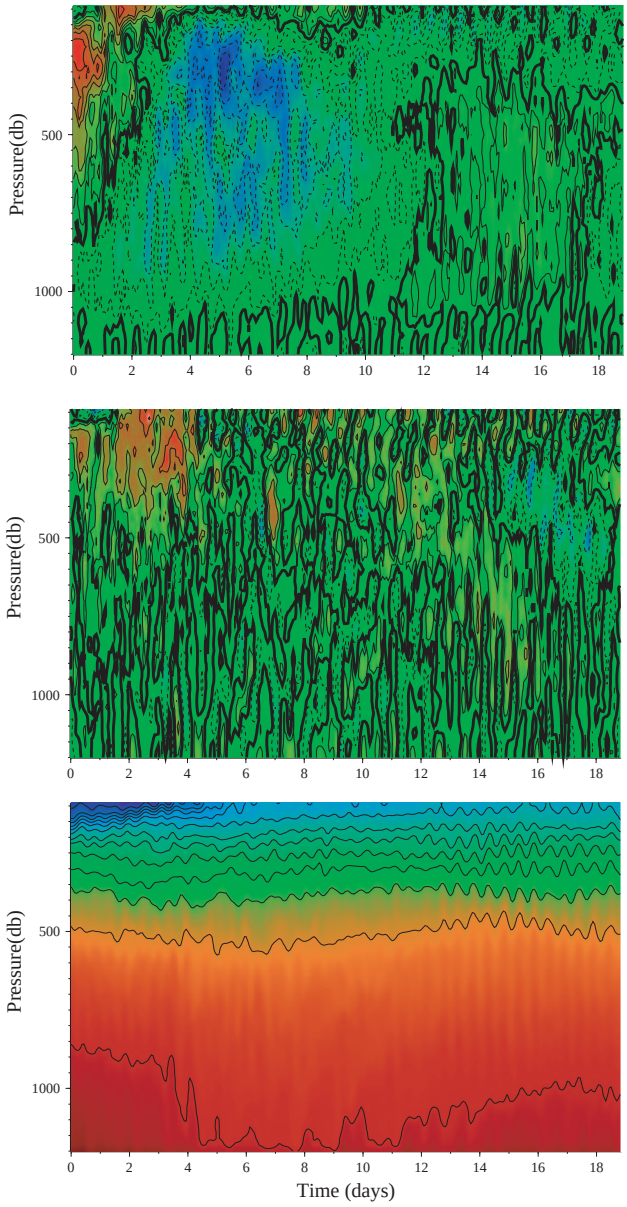

FIG. 3. Contours of 20 m $\times$ 1.5 hr binned Moored Profiler data plotted against time and pressure. Upper panel: Along velocity. Middle Panel: Across velocity. Both panels feature a bold zero contour associated with a green background. Positive values are displayed in red with a solid contour; negative values are displayed in blue with a dashed contour. Lower Panel: Potential density anomaly (σ_θ). The contour interval is 0.05 m s^{-1} for velocity with zero values represented as a thick solid line and 0.25 kg m^{-3} for $\sigma_\theta < 27.00$, 0.125 kg m^{-3} for $\sigma_\theta > 27.00$.

placement field is noted over days 12-18. Nash et al. (2004) interpret data from this time period in terms of the scattering of an incident internal tide.

The tidal band estimates and this interpretation are discussed further in Polzin (in preparation).

d. microstructure

Throughout the field program attempts were made to reoccupy HRP grids about the moored array, Figure 2. Unfortunately, this sampling scheme was interupted by the loss of HRP both prior to and during a time series station (TS1). These grid surveys were further interupted for expendable surveys to the north of the moored array. Despite these interuptions, there is a clear signature of turbulent dissipation (ϵ) in the bottom half of the water column being enhanced by an order of magnitude during

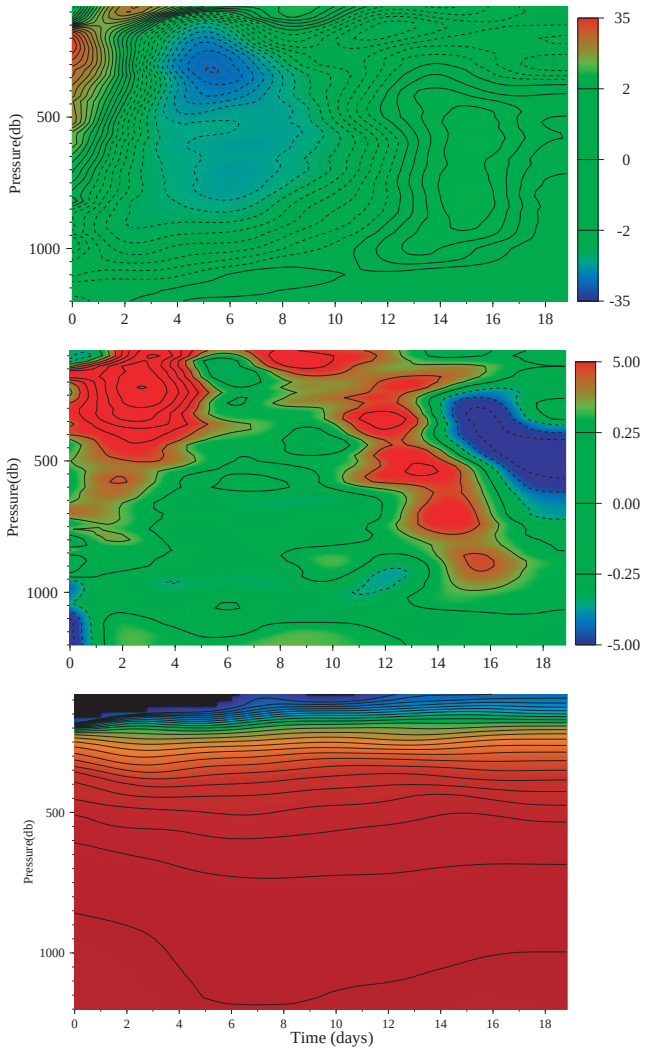

FIG. 4. Contours of low-passed (periods longer than 4.5 days) Moored Profiler velocity plotted against time and pressure. Upper panel: Along velocity. Middle Panel: Across velocity. Both panels feature a bold zero contour associated with a green background. Positive values are displayed in red with a solid contour; negative values are displayed in blue with a dashed contour. Lower Panel: Potential density anomaly (σ_θ). The contour interval is 0.02 m s^{-1} for velocity with zero values represented as a thick solid line and 0.05 kg m^{-3} for the potential density anomaly. *Fix upper left corner of σ_θ plot*

the middle portion of the field program, Figure 7. The increase in dissipation coincides with both the period of strongest flow and the appearence of the subinertial fluctuations.

As the HRP data are somewhat gappy, a Richardson number scheme (Polzin 1996) is used to fill in missing time periods with the MP data. Dissipation associated with turbulent production via shear instability was estimated as:

$$\epsilon_{pseudo} = \delta z^2 \frac{1.76N^3}{96}\left(\frac{S^2}{N^2} - \frac{1}{Ri_c}\right)\left(\frac{S}{N} - \frac{1}{\sqrt{Ri_c}}\right) \quad (1)$$

in which δz represents a first difference interval, $S = (u_z^2 + v_z^2)^{1/2}$ and Ri_c a critical Richardson number. Values of $\delta z = 10$ m and $Ri_c = 1/3$ were used here. An increase in dissipation during the first half of the record is apparent, but the difference is largely an artifact of the color scheme. The average dissipation below 500 m is only a factor of two larger in the first half of the deployment relative to the last.

Not apparent in the pseudo-dissipation records are the order of magnitude larger events in the first L grid and second K grid occupations. These large dissipations are coincident in time with very large amplitude and steep features in the moored density record (Fig. 9). These features couple very weak stratification with positive shear in the across direction during one half of the wave period.

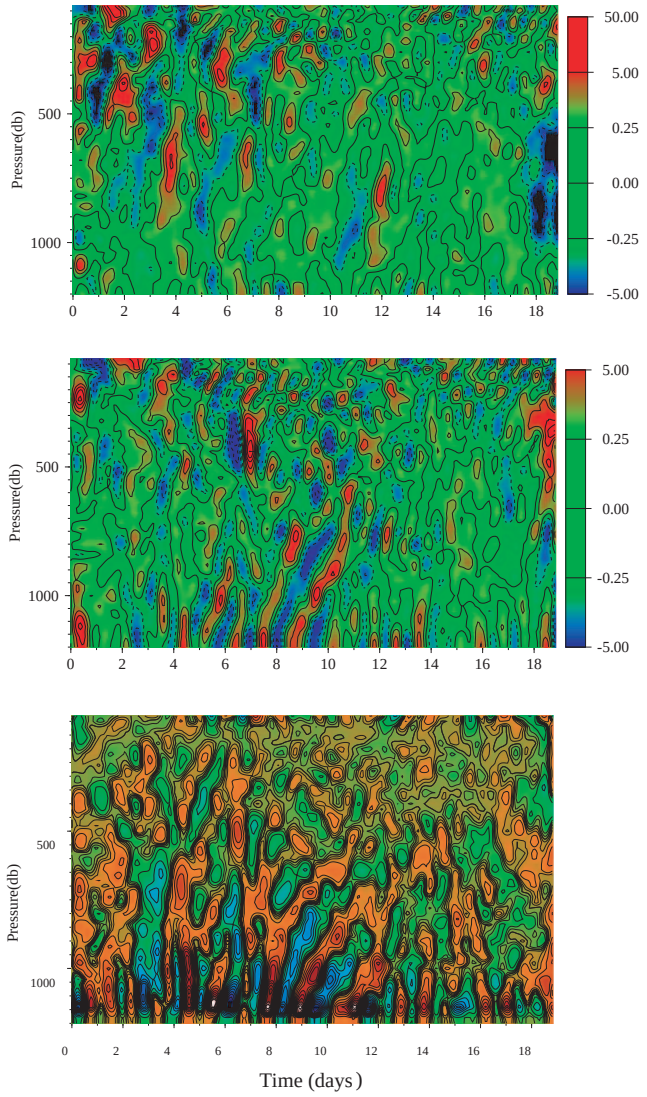

FIG. 5. Contours of band-passed (periods longer than 18 hours but less than 4.5 days) Moored Profiler velocity plotted against time and pressure. Upper panel: Along velocity. Middle Panel: Across velocity. Both panels feature a bold zero contour associated with a green background. Positive values are displayed in red with a solid contour; negative values are displayed in blue with a dashed contour. Note that these band passed velocity amplitudes may be diminshed both by the filtering (a 4-pole Butterworth applied both forwards and backwards) and analyzing the data in a pressure coordinate system. Vertical advection of high wavenumber variability typically Doppler shifts variance to higher frequency and biases the amplitudes to lower values. Lower Panel: Isopycnal displacements estimated from the band-passed potential density anomaly (σ_θ), divided by the low-passed potential density anomaly gradient, ($\partial_z \sigma_\theta$). The contour interval is 0.02 m s^{-1} for velocity with zero values represented as a thick solid line. The displacement contours are 10 m with more closely spaced contours for displacements smaller than 10 m.

The other half period is marked by a very abrupt flow towards shallower water accompanied by denser, stratified water. Such features at least superficially resemble internal bores (ref to Sonya).

The simplest description of this process is that the continental slope represents an internal swash zone. Geostrophy implies that the southward low-passed flow is accompanied by isopycnals which slope downwards in the postive across direction (nominally on slope). Positive across-shear in the wavefield near the bottom tends to advect dense water over light, similar to swash receeding on a beach and encountering shoaling surface waves. Such features are apparent in the HRP stations making dominant contributions to the largest grid averaged dissipations in Fig. 7, Fig. 10.

It may be a coincidence, but the two profiles having

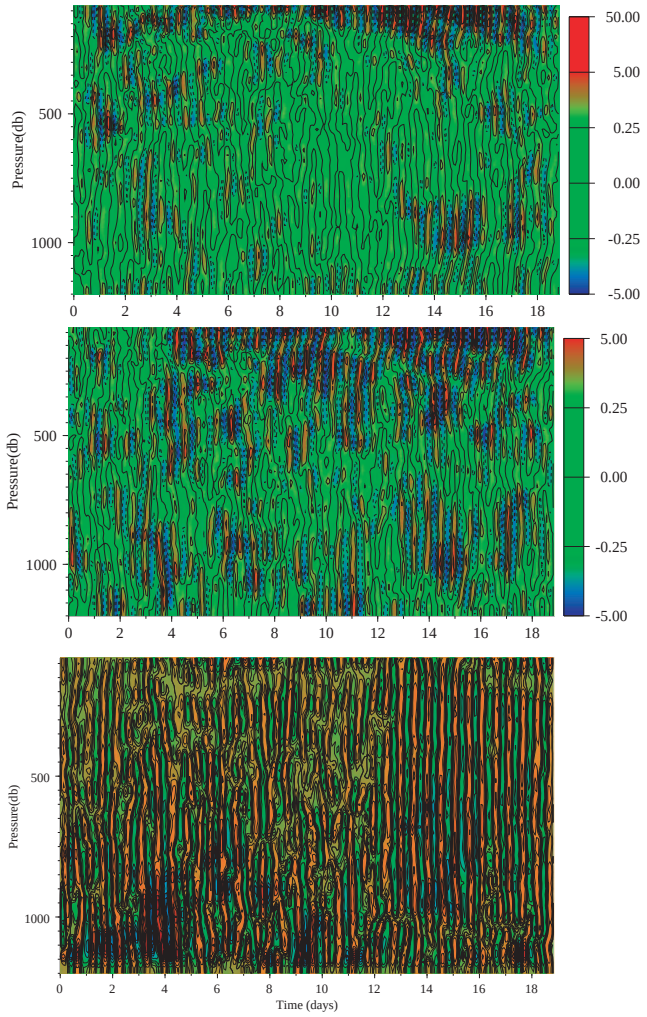

FIG. 6. Contours of tidal frequency (periods between 7.5 and 18 hours) Moored Profiler velocity plotted against time and pressure. Upper panel: Along velocity. Middle Panel: Across velocity. Both panels feature a bold zero contour associated with a green background. Positive values are displayed in red with a solid contour; negative values are displayed in blue with a dashed contour. The contour interval is 0.02 m s^{-1}. Lower Panel: Isopycnal displacements estimated from the band-passed potential density anomaly (σ_θ), divided by the sum of the low- and band-passed potential density anomaly gradients, ($\partial_z \sigma_\theta$). Contours are as in the previous figure.

the largest dissipation rates are located on the lee side of the ridges. Since the moorings are located in the center of a gully, this may explain some difference between the mooring derived pseudo-dissipation estimates and the HRP dissipation rates. Alternately, shear instability might not be the best description of wave breaking in the swash zone.

Are overturns properly dealt with in Figure 8? Probabley not.

3. Budgets

a. Wave Propagation in Geostrophic Shear

This study was initiated as an attempt to understand the sources and evolution of subinertial finestructure and its connection to the coincident enhancement in dissipation. My leading hypothesis is that the subinertial variability is related to the presence of the lower frequency flow field. This then takes us into the quagmire of wave-mean interactions. The intent below is to draw upon only the most general results required to build an appreciation of how the observations *might* be interpreted. It is not the intention to offer a *definative* interpretation.

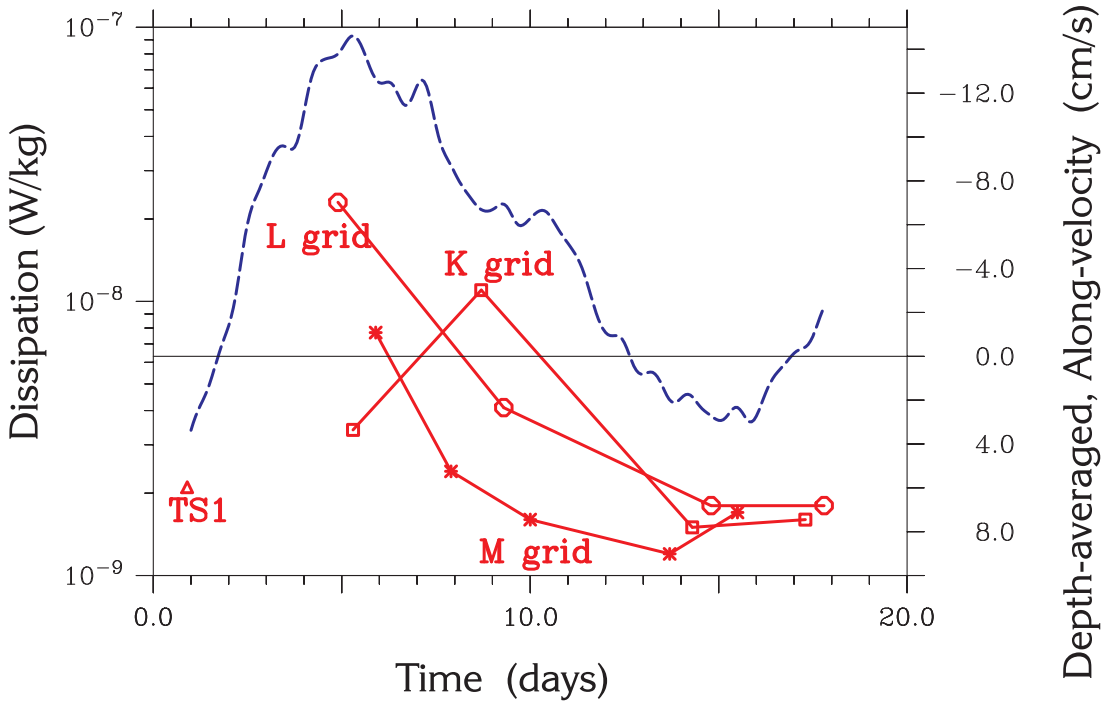

FIG. 7. Symbols denote the average dissipation below 500 db for individual occupations of the grids or time series stations in Figure 1. The low-passed along-slope (positive northward) current below 500 db at the MP array is given by the dashed line. The horizontal axis is time in days since the deployment of the mooring whose data is plotted in Figure 10. Each dissipation estimate is an average over 6 or more HRP profiles. The vertical profiles of turbulent diffusivity ($K_\rho = 0.25\epsilon/N^2$) for the entire field program appear in Figure 1. Due to sampling constraints, the profiles for all but the last two data points are terminated at about 80 m above the bottom. The profiles contributing to the last two data points terminate at about 20 m above the bottom. Given the observed bottom enhancement of the turbulent dissipation, Figure 1, the earlier data are likely biased low.

The point of departure is to note that the wavenumber and frequency estimates indicate the presence of a critical layer at a depth of 500-700 m, Fig. 11. Depending on the estimate of Eulerian frequency (σ), estimates of intrinsic frequency approach zero ($\sigma = 2\pi/24$ hours) or change sign ($\sigma = 2\pi/45$ hours) in the vertical for days 2-11. During this time period, the band-passed currents exhibit a relative minimum in energy at 700 m, Fig. 12. The critical layer is taken to coincide with this energetic minimum.

If one assumes advective effects are minor [$\mathbf{k} = (0, l, m)$], the issue of wave-mean interactions for a parallel [$\overline{u} = \overline{u}(y, z)$] geostrophically balanced background flow becomes much simpler. In this case, freely propgating internal waves have a lower bound (Hoskins 1974) given by:

$$\sigma^2_{min} \cong fQ/N^2 \qquad (2)$$

in which Q is the geostrophic version of Ertel potential vorticity q:

$$q \equiv \frac{f + \nabla \times \mathbf{u}}{\rho} \cdot \nabla\rho$$
$$Q = N^2(f + \zeta) - fS^2 \qquad (3)$$

with $S = \overline{u}_z$ and $\zeta = \overline{v}_x - \overline{u}_y$.

Nondimensional parameters are Froude number $F_r = \sqrt{U_z^2 + V_z^2}/N$ and (Rossby number) $R_o = (V_x - U_y)/f$. Both the low-passed R_o and F_r are not small. Day 2 is characterized by $F_r > 1$ at 1100 m. Days 3-10 and 11-16 are characterized by $R_o < -1$ above 200 m and at depths of 400-900 m, respectively. Consequently there are sign reversals of potential vorticity at various vertical levels during much of the field program. The existence of a sign reversal in potential vorticity is a sufficient criteria for symmetric instability [(Hoskins 1974), (Ooyama 1966)] and thus instability of the low-passed flow field should not be surprising.

However, the presence of a critical layer implies that advective effects are not small. The stability criteria for the general case (both k and l non-zero) (e.g. McWilliams et al. 2001) are ill-defined and the interpretation of the subinertial variability in terms of a specific instability tenuous. What can be said, though, is that the observations document forcing of the wave as it propagates away from the critical layer (subsection b below) and there is an abrupt change in sign of the momentum flux divergence at a level corresponding to highly sheared flow near the

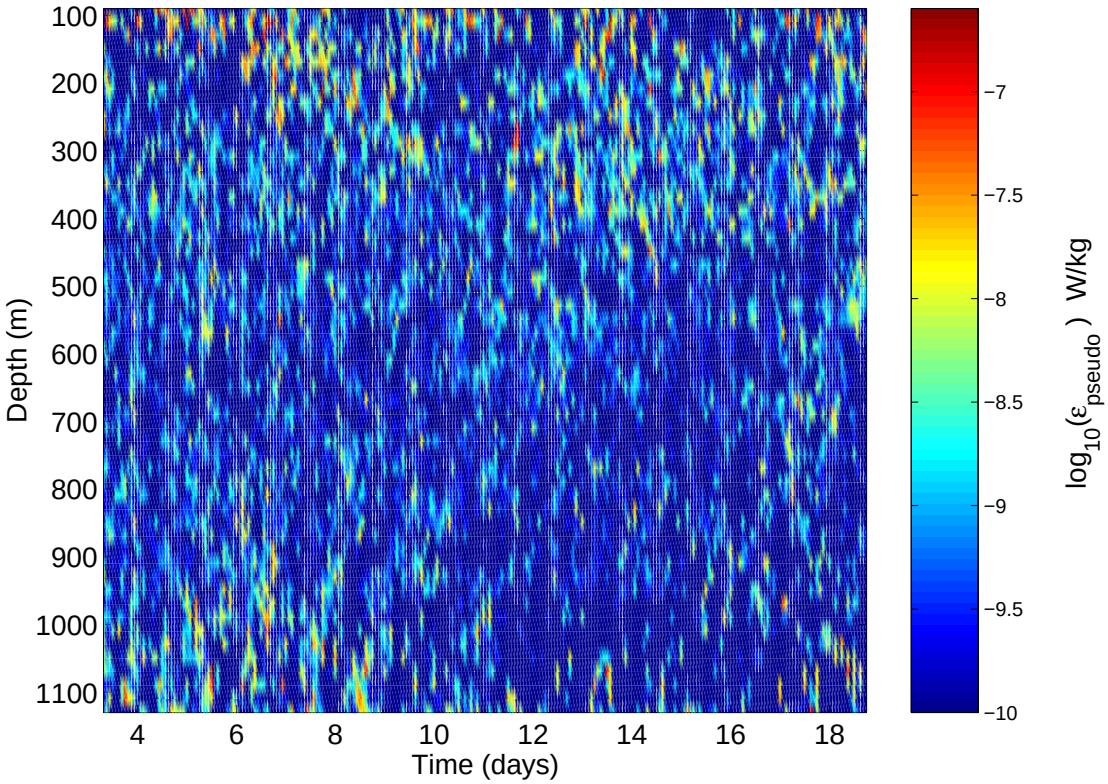

FIG. 8. Pseudo-dissipation record using data from mooring 'B'.

tops of the topographic roughness.

b. Momentum

The usual context for considering wave or eddy interactions with a mean flow is some form of residual theory, consisting of [a basic state $\overline{u}(y,z)$ is again assumed] equations for:

the residual mean momentum $\overline{v}^{\dagger}$

$$\overline{u}_t - f\overline{v}^{\dagger} = \rho_o^{-1}\nabla\cdot\mathbf{F} + \frac{\partial\chi}{\partial z} \tag{4}$$

f is the Coriolis parameter, $\overline{v}^{\dagger}$ an ageostrophic residual normal to $\overline{u}$, $\overline{u}_t$ indicates the tendancy of the background velocity field, $\mathbf{F}$ the Eliassen-Palm flux (Eliassen and Palm 1961), and χ a mean drag associated with non-wavelike stresses. Here there has been no assumption about the size of R_o or F_r, only that the background is in geostrophic balance, and no assumption about small amplitude fluctuations has been made.

The residual $\overline{v}^{\dagger}$ is defined so that steady linear non-dissipative waves, for which $\nabla\cdot\mathbf{F}=0$, cannot result in a mean acceleration: $\overline{u}_t = \overline{v}^{\dagger} = 0$; the Charney-Drazin non-acceleration theorem (Charney and Drazin 1961).

The Eliassen-Palm flux represents a radiation stress associated with inviscid waves in a stratified rotating fluid. The Eliassen-Palm flux can be thought of as a *general relationship* linking both internal gravity waves **and** planetary waves to the structure of the background that provides their restoring force. The Eliassen-Palm flux, for a background flow [$\overline{u} = \overline{u}(y,z)$] in the β-plane approximation, is

$$\rho_0^{-1}\mathbf{F} = [0\ ,\ \overline{u}_z\overline{v'\rho'}/\rho_{0z} - \overline{u'v'}\ ,\ (f-\overline{u}_y)\overline{v'\rho'}/\rho_{0z} - \overline{u'w'}] \tag{5}$$

(Eliassen and Palm 1961). At small amplitude, the Eliassen-Palm flux represents the flux of pseudo-momentum,

$$\mathbf{F} = \mathbf{C_g}\cdot\frac{\mathbf{k}E}{\omega} \tag{6}$$

EP estimates: be sure to include band-passed $\overline{u}_y$, $\overline{u}_z$ gradients. Don't trust the estimate of vertical velocity in estimating the vertical EP flux below 800 m for moorings 'B' or 'C' as horizontal gradients are not well resolved in the array below that depth. Does uw make much contribution to the flux?

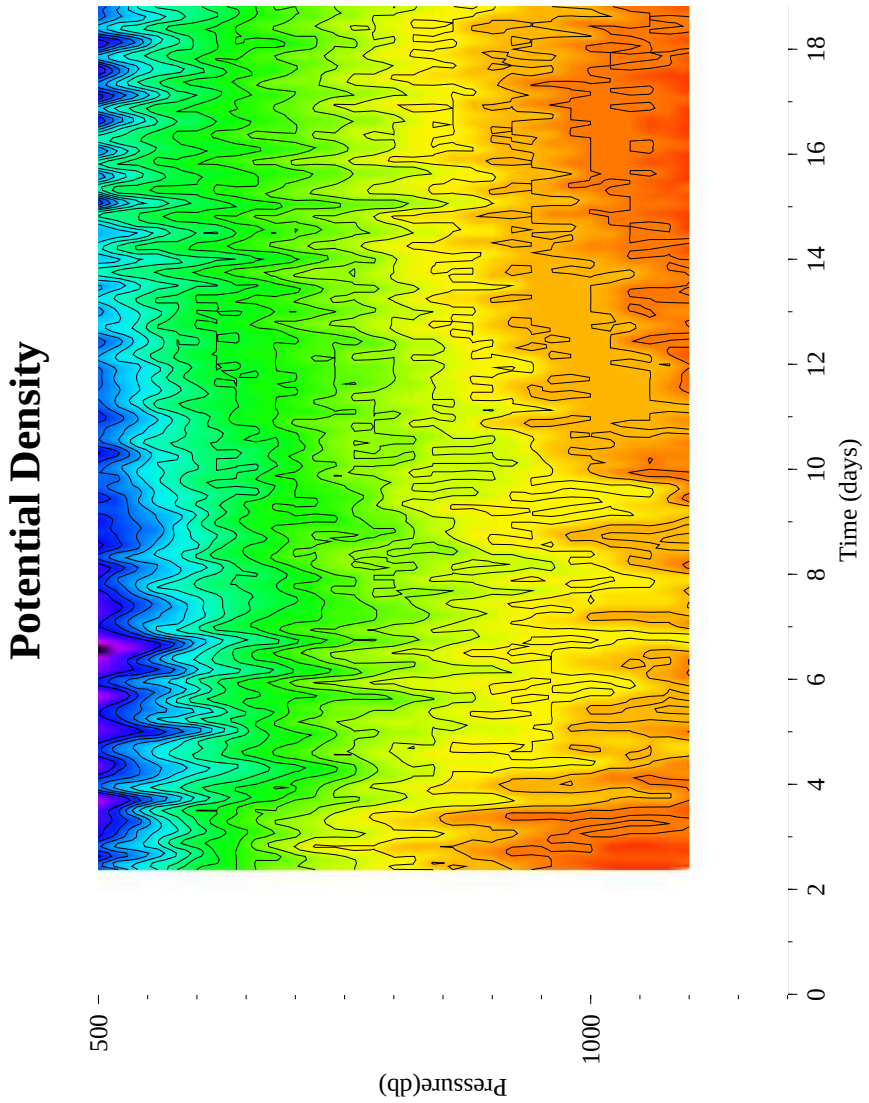

FIG. 9. Densely contoured density field from mooring 'C'. *Add boxes at days 4 and 6-8 to mark large amplitude waves. Adjust the time axis on this plot! What is contouring interval?*

The band-passed estimates of the vertical flux, F^z, are near zero above 700 m and decrease towards to values of $3 - 4 \times 10^{-5}$ m^2 s^{-2} at 1100 m. An increasing vertical flux with height above bottom is in the sense of providing

a positive (ñorthward) acceleration to the negative low-pass along velocity. The deepest two moorings indicate a reversing trend so that near bottom values are close to zero. This decreasing flux with height is in the sense of providing a negative (ŝouthward) acceration to the negative low-pass along velocity.

The band-passed horizontal fluxes are negative at 400 m and positive at 1000 m.

The horizontal fluxes associated with the low-passed records are typically larger than the band-passed fluxes by an order of magnitude. However, it is not clear how to interpret averages over what may be only a fraction of an event.

c. Energy

Consider an energy equation consistent with the residual formalism:

$$\frac{\partial E}{\partial t}+\overline{u}\cdot\nabla E+\nabla\cdot p'\mathbf{u}' = (F^y\overline{u}_y+F^z\overline{u}_z)+S_o-S_i+N.L. \tag{7}$$

In order of appearance the terms are: [1] energy tendancy, [2] advection, [3] energy flux, [4&5] the rate of work done by the radiation stress on the background, [6] sources, [7] sinks and [8] nonlinearity.

Here direct estimates of [1] the tendency, [4&5] the rate of work (given as the product of the momentum flux and gradients in the background) and [7] dissipation ($S_i = (1+R_f)\epsilon$, with $R_f = 0.2$ expressing the partition of turbulent production into dissipation (ϵ) and a buoyancy flux) are available. Vertical flux divergences [2]&[3] are assumed to be zero at both the lower boundary and the critical layer so that the depth mean (1200-700 m) is zero. Horizontal flux divergences are not robust as the mooring array is not sufficiently extensive.

Direct estimates of the subinertial source and nonlinearity are not available.

[Tendency $O(\pm 2\times 10^{-9}$ W/kg]

.

[Work $O(-5\times 10^{-8}$ W/kg]

.

[Dissipation $< O(-1\times 10^{-8}$ W/kg]

.

[Source of $O(+5\times 10^{-8}$ W/kg] required to balance.

S_o as $\Im(\sigma)E$, $\Im(\sigma)\cong f$

.

$KE/PE \cong 1.$ but note difference with APE - tilted isopycs.

d. Potential Vorticity

Do Ageostrophic version of PV for band-passed field. Also low-passed.

Discuss PV figures

div F = PV flux in QG approximation. How about in general?

A central construct of Geophysical Fluid Dynamics is potential vorticity dynamics. In the quasi geostrophic approximation, the E-P flux divergence is equal to the potential vorticity flux. Here, the vertical E-P flux gradient is $O(10^{-7})$ m s^{-2}, or $O(10^{-3})$ m s^{-1} when normalized by the quasi-geostrophic potential vorticity of f. The Ertel potential vorticity flux is $O(10^{-11})$ m s^{-4}, or $O(10^{-2})$ m s^{-1} when normalized by the Ertel potential vorticity of $f\overline{N^2}$.

4. Summary

These observations are obvious fodder for further theoretical and numerical work and call for further field programs to explore the phenomena.

High wavenumber fluctuations appear with mean flow. Their identity *vis* sub- and super-inertial dynamics is obscure because of time dependence and large gradients associated with the mean flow. The background fields are not documented well enough to permit a definative comparison to any simple analytic construct.

One characterization of these data is in terms of strongly stratified rotating turbulence. This characterization is supported by the observations of the low-passed flow having $R_o, F_r \sim O(1)$) and sign reversals of potential vorticity, a parameter range characteristic of strongly stratified, rotating turbulence (REF). This characterization could be appropriate for the upper part of the water column, in which the subinertial variability lacked appreciable spatial and temporal coherence.

This paper focussed upon subinertial variability in the

lower part of the water column which was characterized by coherent phase relations. An interpretation in terms of a nearly monochromatic wave structure and critical layer phenomena was pursued.

This system is seriously complicated and a description in terms of small parameter expansions and weak nonlinearity is seriously strained. Thus the discussion focused upon qualitative exposition rather than quantitative prediction. I feel that the later is premature given uncertainty in our dynamical understanding of the sytstem's behavior. Thus even this attempt at describing the possible behaviour of the system might be a useful foil for further theoretical studies.

The field program was intended to investigate quasi-stationary internal lee waves set up in response to flow over roughness superimposed upon the continental slope. Quasi-stationarity would imply that the internal wavefield would evolve with Eulerian frequencies of the geostrophic field. This was not found. Rather, the time dependence was much stronger. The observed finestructure was interpreted as the result of an instability associated with the highly sheared flow field. Why was this flow so highly sheared? An immediate answer is that the lee wave field had sufficient amplitude to break immediately next to the boundary, providing an initial drag that set up the shear, which in turn produced the instability.

The resulting momentum flux profile set up by wave dynamics provides a boundary layer structure that extends hundreds of meters away from the boundary. This is far in excess of the height scale typically associated with viscous stresses above a planar boundary. An additional complication is that the effective bottom boundary conditions for the low-passed flow field may be significantly altered as well.

In terms of energetics, the work done by the waves against the background flow likely participates in a dominant balance with forcing by the instability. The energy tendency and dissipation are small in comparison. Growth rates of the instability are inferred to be $O(f)$.

Band-passed Ertel potential vorticity fluxes are 0.01 $f\overline{N^2}$, significantly larger than $\partial_z F \cong 0.001 f$. The quasi-geostrophic potential vorticity flux is expected to be equal to the E-P flux divergence.

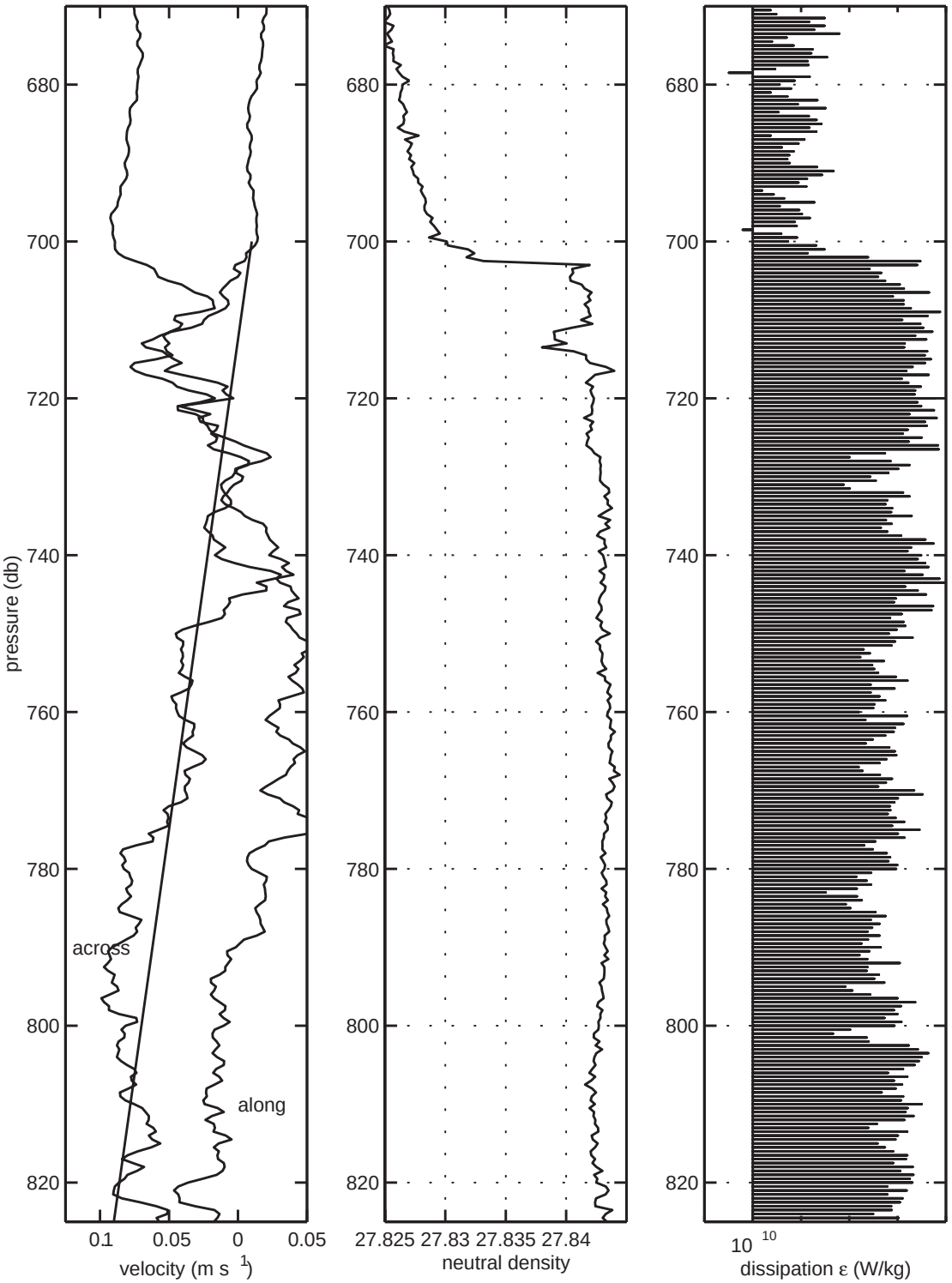

FIG. 10. HRP profile from the first occupation of the 'L' grid. The profile is terminated about 60 m above the bottom. *It could be worth while resorting the velocity and density profiles, then calculating the shear instability production terms with sorted gradients.*

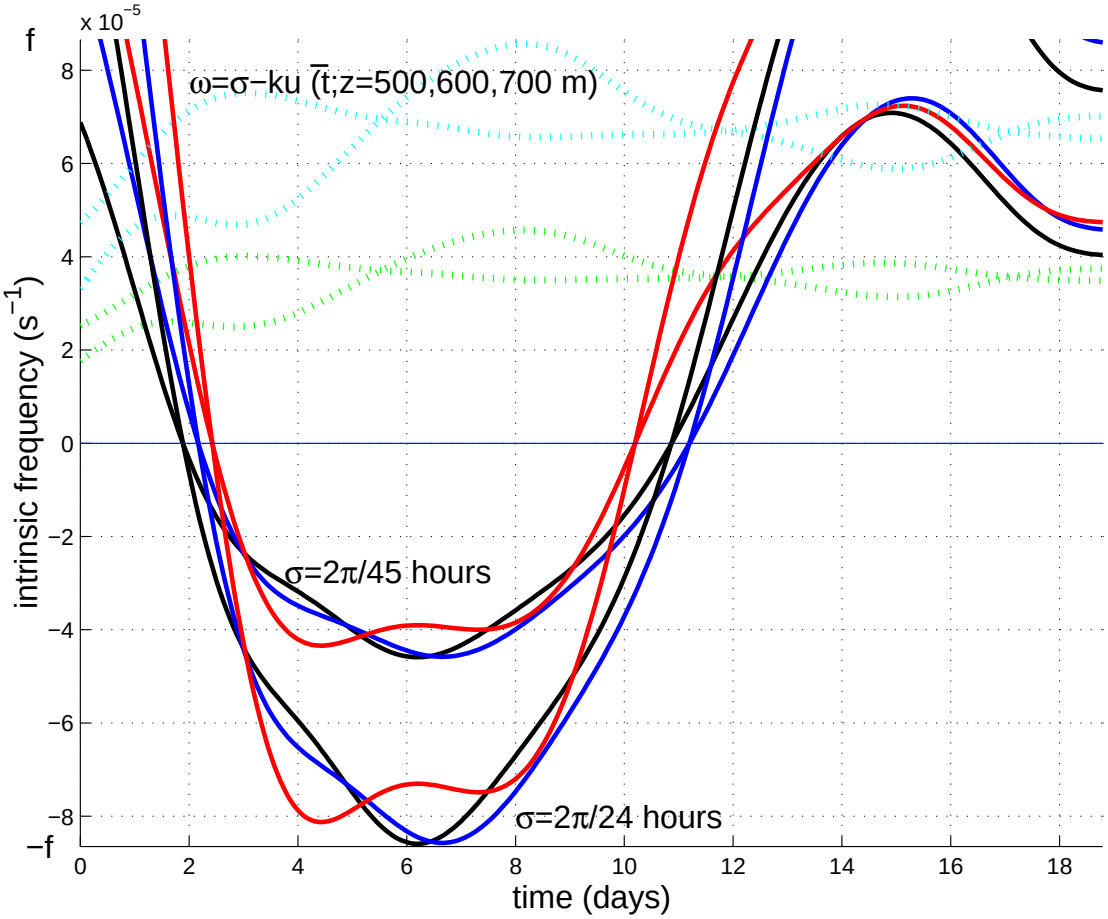

FIG. 11. Time series of intrinsic frequency $\omega = \sigma - k\overline{u}$ for two estimates of the dominant Eulerian frequency σ and low passed currents at 500, 600 and 700 m depth. The estimates bound the value of $\omega = 0$ for days 4-11 and thereby indicate the presence of a critical layer at that depth.

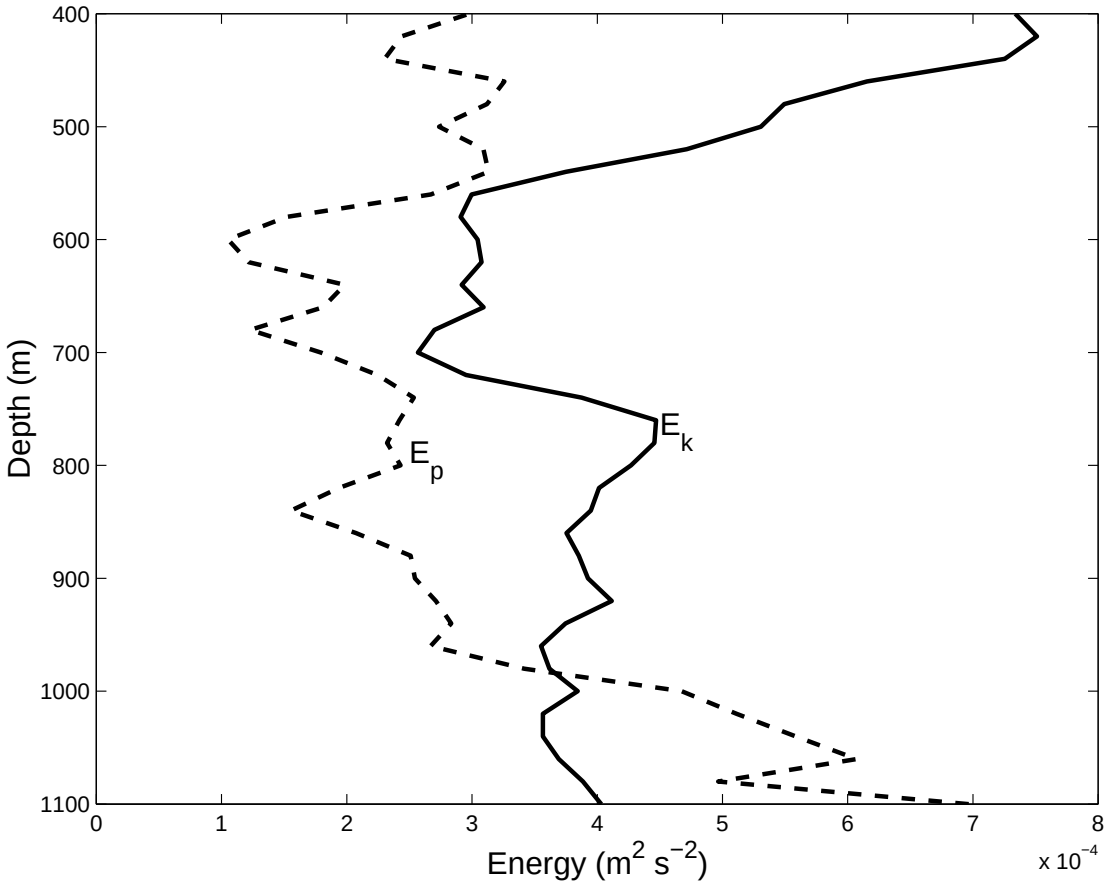

FIG. 12. Estimates of band-passed kinetic E_k and potential E_p energy averaged over days 4-11. Note the presence of an energetic minimum at 600 m, the depth of the critical layer identified in the previous figure.

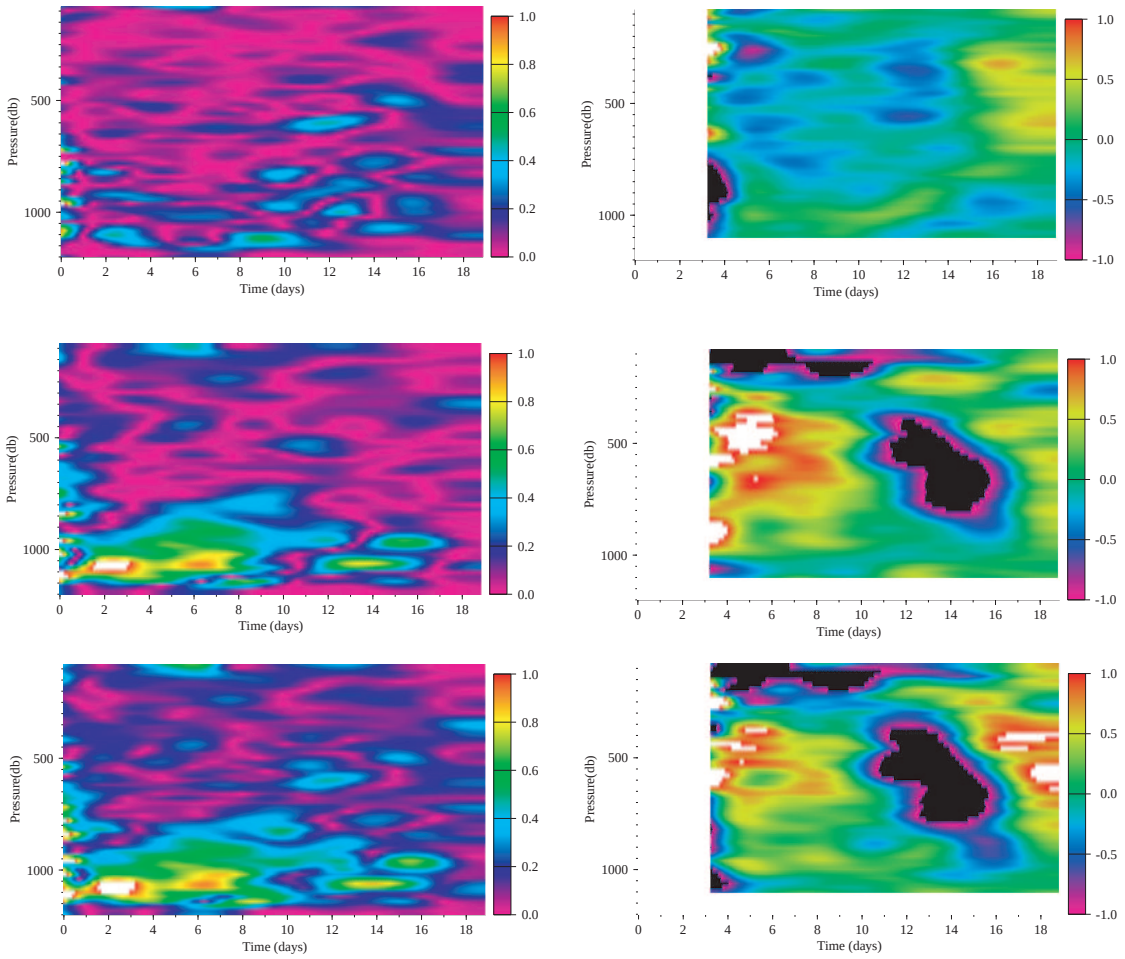

FIG. 13. Time-depth series of across shear $\mid \overline{v}_z/N \mid$, along shear $\mid \overline{u}_z/N \mid$, Froude number $(\overline{v}_z^2 + \overline{u}_z^2)^{1/2}/N$, vorticity $\overline{v}_x/f$, $-\overline{u}_y/f$ and and $(\overline{v}_x - \overline{u}_y)/f$ estimated from the low-passed velocity and density fields.

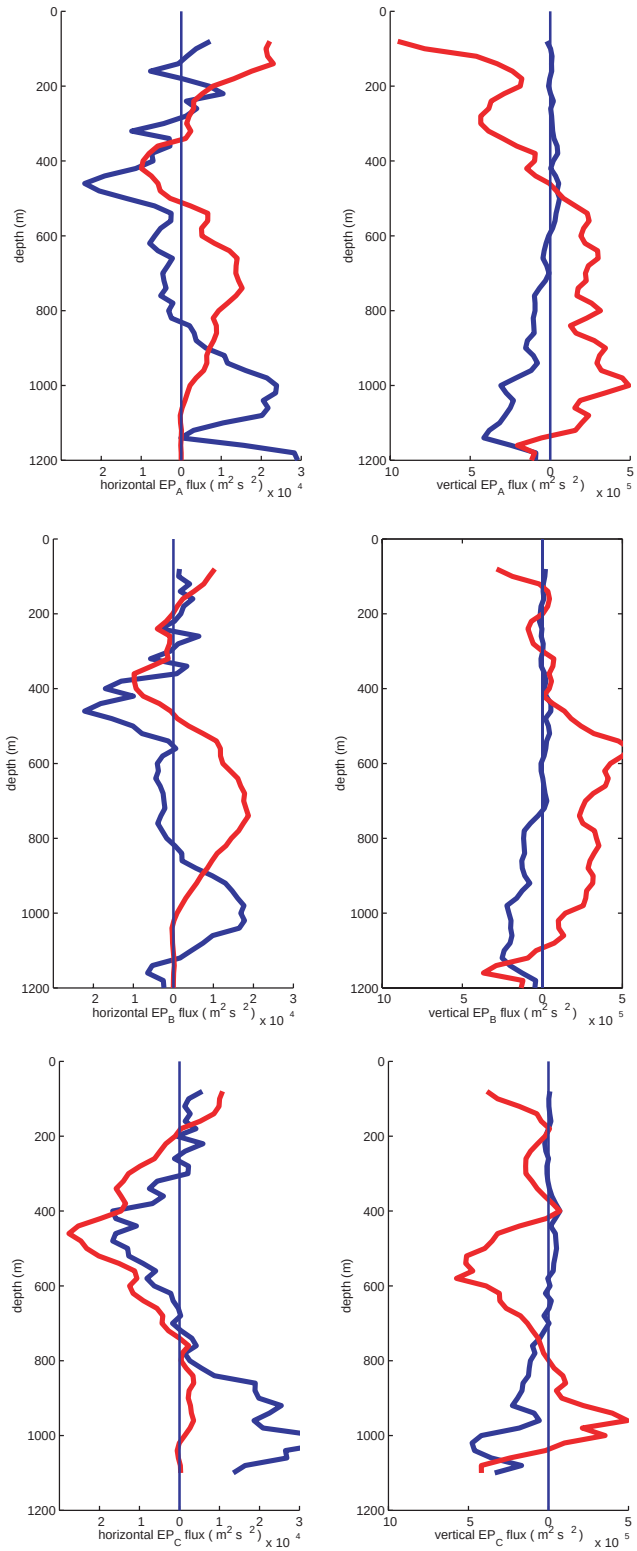

FIG. 14. Mean (averaged over mooring 'B' deployment, excluding the first and last days) Eliassen-Palm fluxes for low- and band-passed fluctuations versus depth. Moorings 'A' 'B' 'C'.

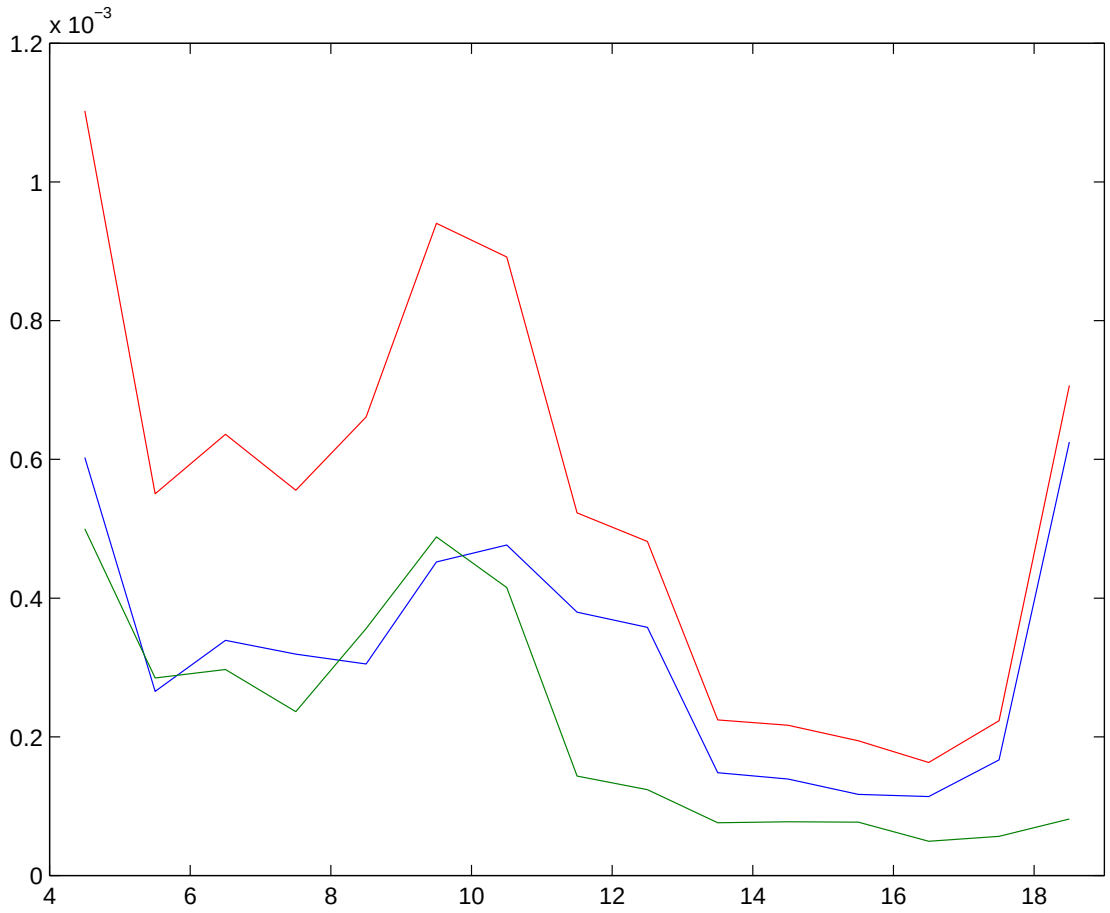

FIG. 15. Estimates of band-passed kinetic E_k and potential E_p energy averaged over 600-1100 m depth. Note the presence of an energetic maximum on day 10.

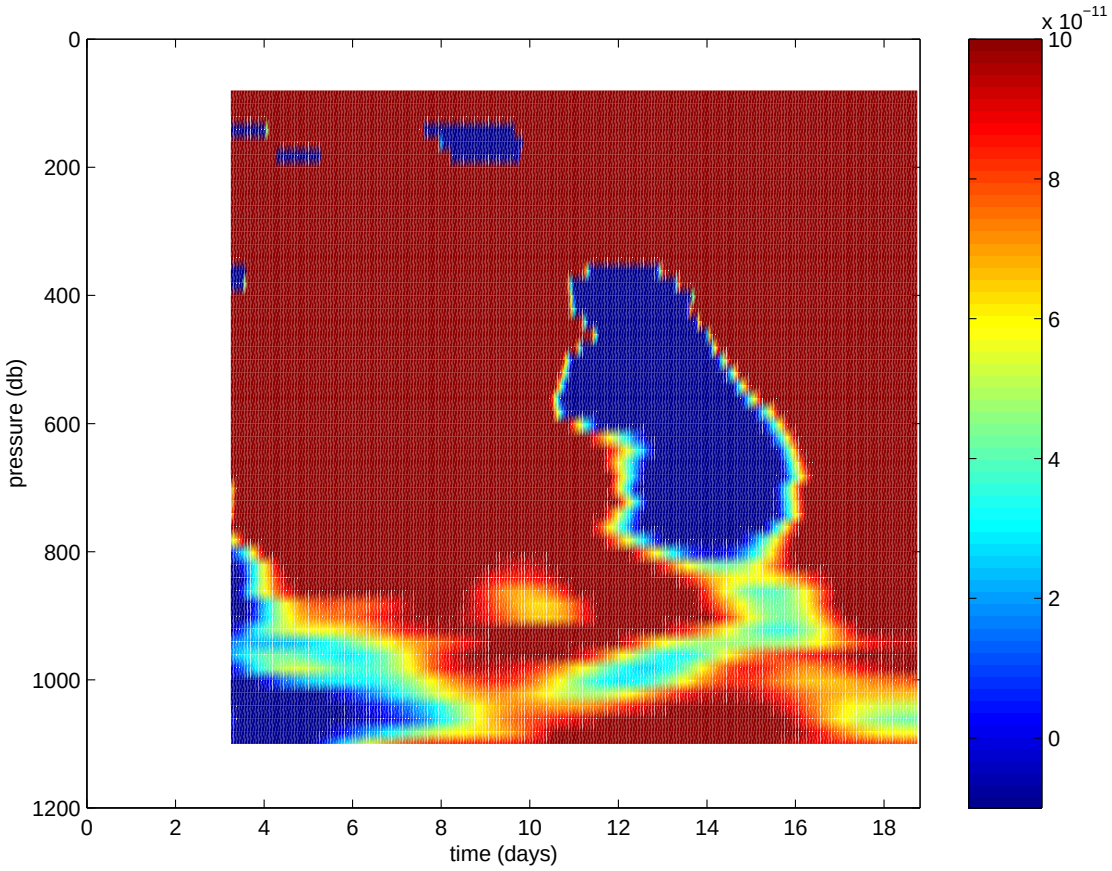

FIG. 16. Time-depth series of low-passed Ertel potential vorticity.

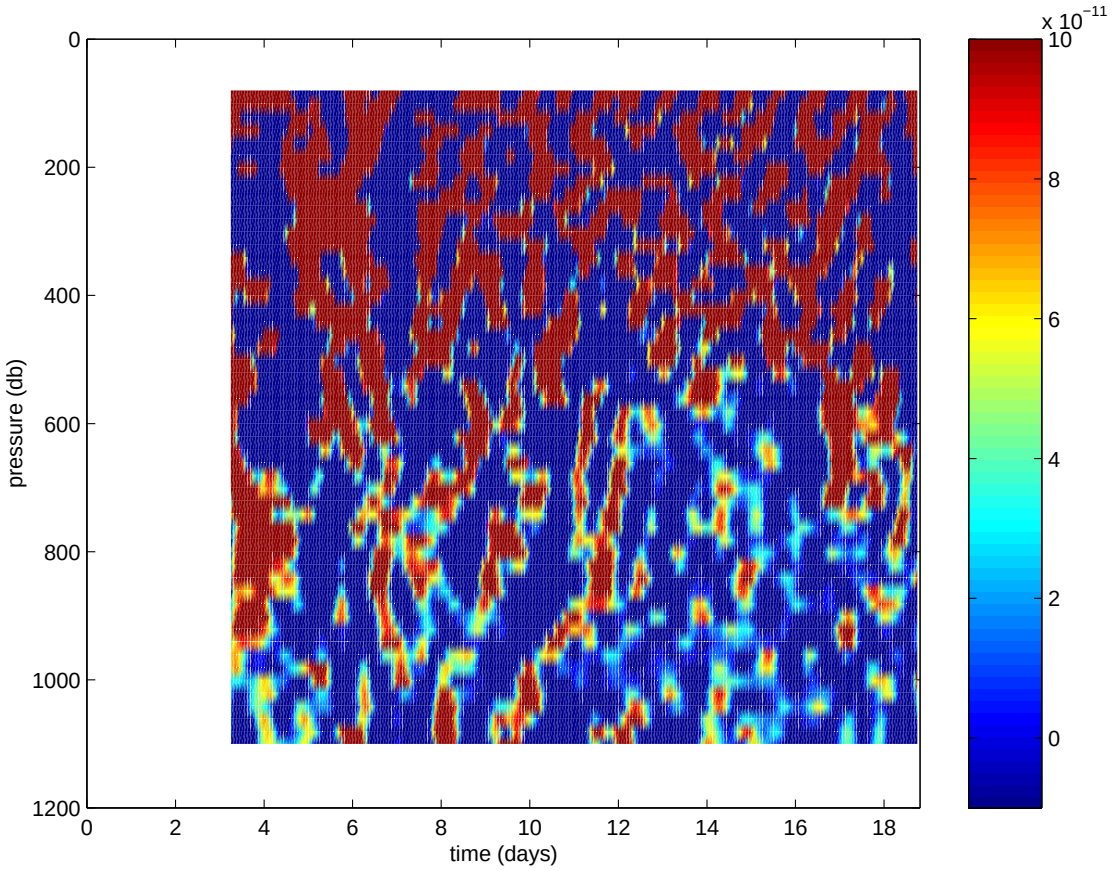

FIG. 17. Time-depth series of band-passed Ertel potential vorticity.

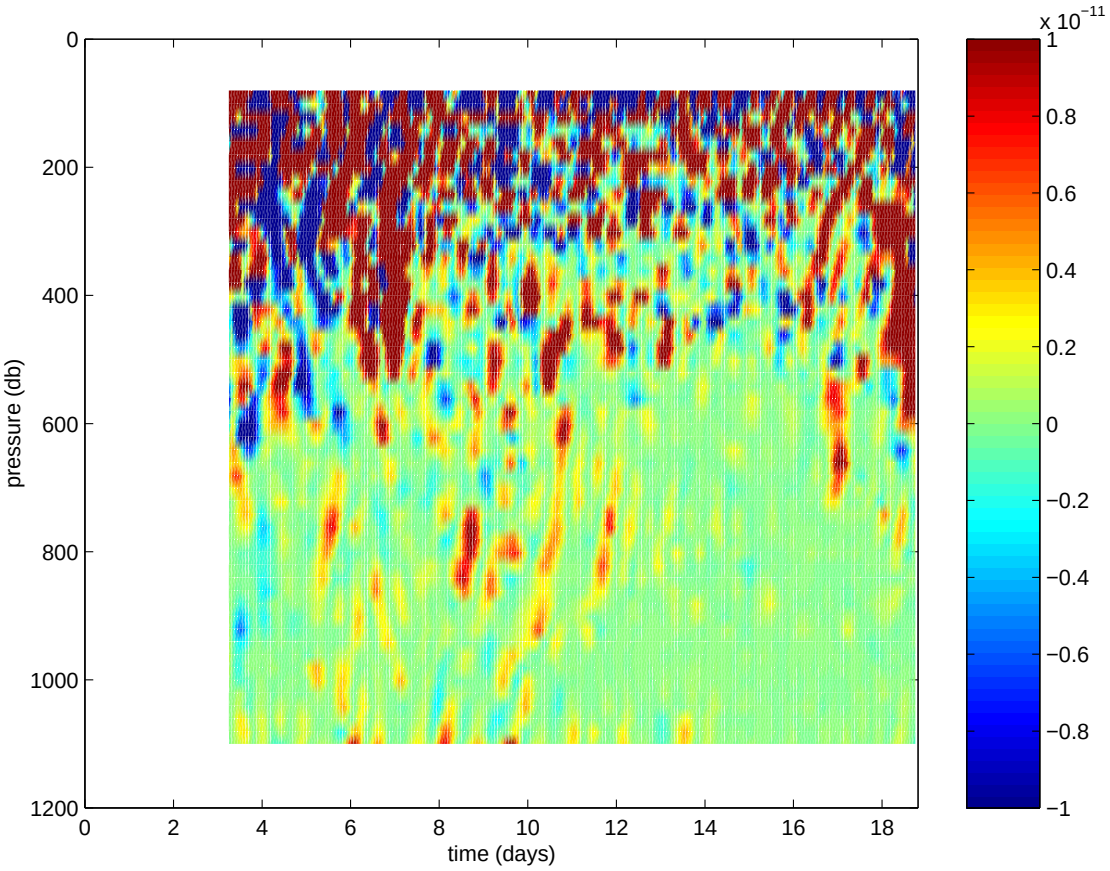

FIG. 18. Time-depth series of band-passed potential vorticity flux, $\overline{v'q'}$.

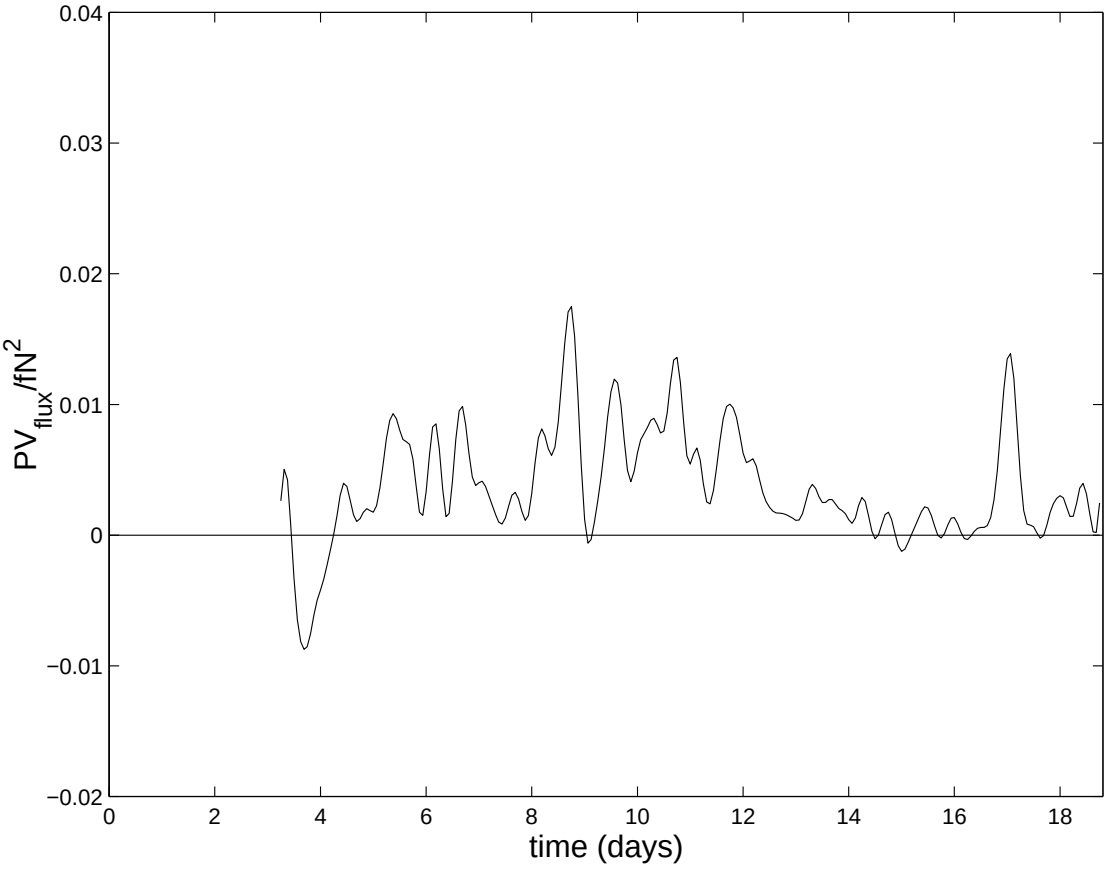

FIG. 19. Time series of band-passed potential vorticity flux divided by $f\overline{N^2}$.

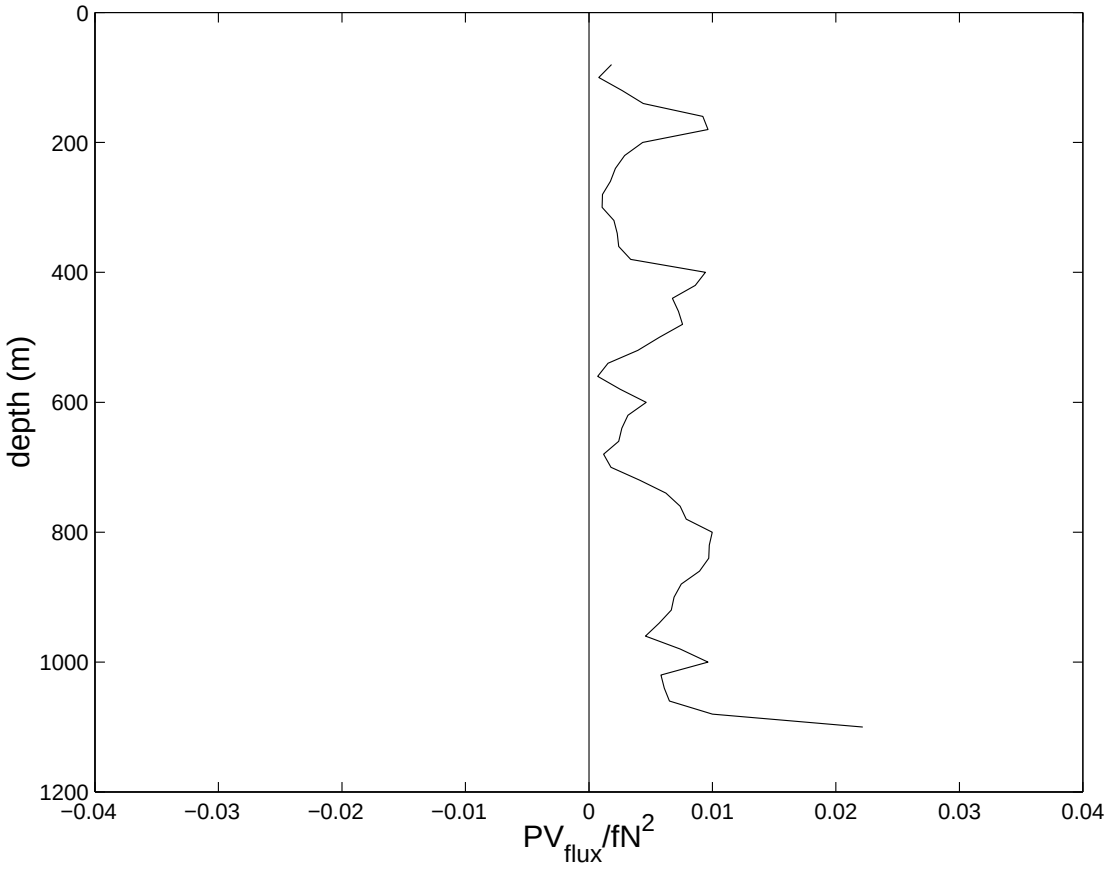

FIG. 20. Depth profile of band-passed potential vorticity flux divided by $f\overline{N^2}$.

Acknowledgements. Like many oceanographic instruments, the High Resolution Profiler is one-of-a-kind. Our cruise preparations were complicated by an explosion within its pressure case, apparently triggered by a faulty battery. After the battery blew up on April 23, it was not clear that the HRP could be repaired, let alone repaired in time to meet the May 10 departure schedule. That the cruise took place as scheduled is due to the dedication and experience of many people in the greater WHOI community. Significant engineering support and assistance in testing were contributed by Marshall Swartz, Steve Liberatore, Dick Koehler and Al Fougere. Assembly assistance and spare parts were obtained from Karlen Wannop, Jim Valdes's group and Craig Taylor. John Toole's efforts with the MP development and data analysis were invaluable. Raffaele Ferrari demonstrated the utility of residual-mean theory to the author. Finally, I gratefully acknowledge the support and patience of ONR during the acquisition and analysis of these data.

APPENDIX A

Appendix

a. Topographic Waves

The simplest model geometry for topographic edge waves in a rotating stratified fluid consists of a infinite planar slope. The situation is highly idealized, of course, when it comes to discussing the oceanic observations as such a model neglects variations in topographic slope and the presence of the sea surface. But such a simplified model serves to point out several basic features of edge waves, such as: (1) rectilinear polarization of the wave motions, (2) phase and group propagation, (3) the evanescent nature of the topographic waves, and (4) provides a dispersion relation. The discussion below directly follows that in Rhines (1970).

Consider a planar slope inclined at an angle α to the y–axis such that the plane is given by $z = y\tan(\alpha)$. After rotating the (x, y, z) coordinate system into this plane and then rotating about the new z axis by an angle ϕ (positive clockwise), solutions having the spatial dependence of $exp[(-\kappa + ik_3)x_3 + i(k_2x_2 - \sigma t)]$ can be obtained, in which (x_1, x_2, x_3) is the new coordinate system with x_3 normal to the plane and the velocity in the x_2 and x_3 directions vanishes, i.e. $u_2 = u_3 = 0$. For this solution,

$$\sigma = \pm N\sin(\alpha)sin(\phi) \tag{A1}$$

$$\frac{\kappa}{k_2} = \frac{S[1-\sin^2(\alpha)\sin^2(\phi)]}{\cos^2(\alpha)+S^2\sin^2(\alpha)\cos^2(\phi)} sgn[\sin(\alpha)\sin(\phi)] \cong S \tag{A2}$$

$$\frac{k_3}{k_2} = \frac{1}{2}\frac{(1-S^2)\sin(2\alpha)\cos(\phi)}{\cos^2(\alpha)+S^2\sin^2(\alpha)\cos^2(\phi)} \cong \frac{-\alpha S^2}{1+S^2\alpha^2} \tag{A3}$$

with $\sigma > 0$, $S = N/f$, N is the buoyancy frequency and f the Coriolis frequency. The following properties of this solution are apparent:

• The motions are rectilinearly polarized in the x_1 direction as $\mathbf{u} = (u_1, 0, 0)$. The highest possible frequency edge wave is $\sigma = \pm N\sin(\alpha)$ ($\phi = \pi/2$), for which the velocities are aligned in the across direction and decay in the normal direction. This highest frequency may well be larger than f.

• The motions are trapped in the direction normal to the slope for $\kappa > 0$. For small topographic slopes and strong stratification, the decay scale relative to the normal wavenumber is given by $\kappa/k_3 \cong -1/S\alpha\cos(\phi)$.

• From (A2), k_2 has the same sign as $sgn[\sin(\alpha)\sin(\phi)]$, so that the phase propagates along an isobath with shallow water to the right. The group velocity is in the same sense.

The ratio of horizontal kinetic to available potential energy, HKE/APE, for a single topographic edge wave is simply:

$$\frac{HKE}{APE} = \frac{\sigma^2}{N^2\tan^2\alpha} = \cos^2\alpha\sin^2\phi \tag{A4}$$

Discuss apparent character of subinertial motions and compare to the simple predictions delineated above.

topographic slope, lambda H, vs x and p N, etc. go larger perspective in topography - ?

Could get elliptical polarization from two waves.

The waves characterized by (A1-A3) are simply buoyancy oscillations. If the topography is non-uniform, for example a non-planar geometry in an unbounded ocean or simply an ocean of finite depth, the variable topography acts as an additional restoring force through vortex stretching. For such waves, the polarization relations and dispersion relation change. The coupled (stratification plus variable topography) problem does not admit to such simple analysis as that presented above (see, for example, Wang and Moores). However, it appears that the analoge of westward phase propagation and trapping to the sloping boundary are retained.

Note: Oscillatory response not apparent unless $S\alpha \gg 1$, for which $\mid k_3 \mid / \mid \kappa \mid = S\alpha\cos(\phi)$, with $\alpha \ll 1$. If $\phi \cong \pi/2$, $\mid k_3 \mid / \mid \kappa \mid = S\sin(2\alpha)(\pi/2 - \phi)$, which is not oscillatory. That is, fluctuations towards the highest permitted frequencies are simply bottom trapped.

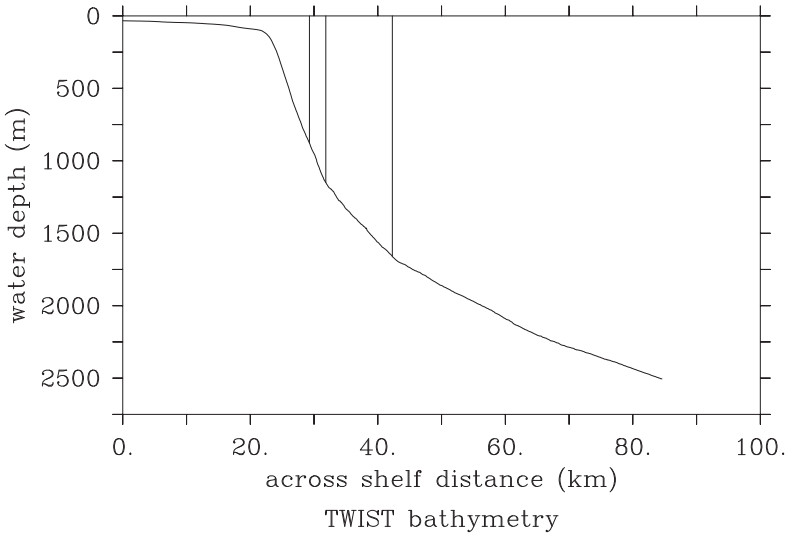

FIG. A1. Along averaged profile of bathymetry vs across distance. The vertical lines delimite the position of N^2 profiles in Figure A2. *Add in moored array and C's? Shelf break origin?*

Table 1: Phase relations of topographic edge waves.

$p>0$	$\phi<0$	$\sigma<0$	$k_2<0$	$\frac{k_3}{k_2}<0$	$westward\&downwardphase$	$bottomtrapped$
$p>0$	$\phi<0$	$\sigma>0$	$k_2>0$	$\frac{k_3}{k_2}<0$	$westward\&upwardphase$	$surfacetrapped$
$p<0$	$\phi>0$	$\sigma<0$	$k_2>0$	$\frac{k_3}{k_2}<0$	$eastward\&downwardphase$	$bottomtrapped$
$p<0$	$\phi>0$	$\sigma>0$	$k_2<0$	$\frac{k_3}{k_2}<0$	$eastward\&upwardphase$	$surfacetrapped$

subsectionDerivation of the Wave Equation
Here is the recipe for deriving the wave equation (**??**):

- Solve (2.4) for w.
- Eliminate w from (2.1)-(2.3).
- Solve (2.2) for u.
- Eliminate u from (2.1) and (2.3).
- Solve (2.1) for v.
- Eliminate v from (2.3).

Note that only the penultimate step involves dividing by a quantity that might possibly be zero (β) for stably stratified flows at mid-latitudes.

REFERENCES

[Baines 1982] Baines, P.G., 1982: On internal tide generation. *Deep-Sea Res.*, **29**, 307-338.

[Doherty et al. 1999] Doherty, K. W., D.E. Frye, S.P. Liberatore, and J. M. Toole, 1999: A moored profiling instrument. *J. Atmos. Oceanic Tech.*, 16, 1816-1829.

[Egbert and Ray 2000] Egbert, G.D. and R.D. Ray, 2000: Significant dissipation of tidal energy in the deep ocean inferred from satellite altimeter data. *Nature*, **45**(6), 775-778.

[Halkin and Rossby 1985] Halkin, D. and T. Rossby, 1985: The structure and transport of the Gulf Stream at 73W. *J. Phys. Oceanogr.*, **15**, 1439-1452.

[Hoskins 1974] Hoskins, B.S., 1974: The role of potential vorticity in symmetric stability and instability. *Q. J. Royal Met. Soc.*, **100**, 480-482.

[Kunze 1985] Kunze, E., 1985: Near-inertial wave propagation in geostrophic shear. *J. Phys. Oceanogr.*, **15**, 544-565.

[Ledwell et al. 2000] Ledwell, J. R., E. T. Montgomery, K. L. Polzin, L. C. St. Laurent, R. W. Schmitt, and J. M. Toole, 2000: Evidence for enhanced mixing over rough topography in the abyssal ocean. *Nature*, **403**(6766), 179–182.

[Montgomery and Polzin 1999] Montgomery, E. T. and K. L. Polzin, 1999: Turbulence and Waves Over Irregularly Sloping Topography: Cruise Report - *Oceanus 324*, WHOI-99-16, Woods Hole Oceanographic Institution, Woods Hole Ma., pp 42.

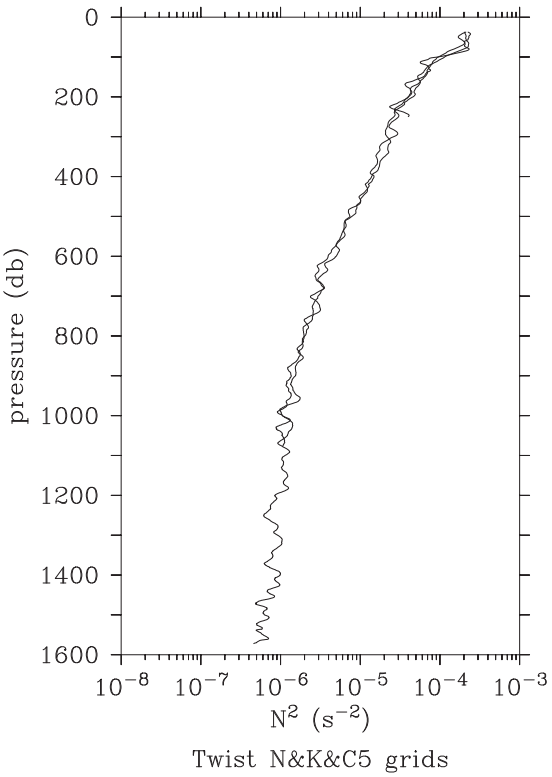

FIG. A2. Vertical profiles of buoyancy frequency squared.*they represent averages over what time period?*

[Munk 1997] Munk, W., 1997: Once again: once again–tidal friction. *Prog. Oceaogr.*, **40**, 7-35.

[Ooyama 1966] Ooyama, K., 1966: On the stability of the baroclinic circular vortex: a sufficient criterion for instability. *J. Atmos. Sci.*, **23**, 43-53.

[Pedlosky 1982] Pedlosky, J, 1982: Geophysical Fluid Dynamics. Springer Verlag, New York, pp. 624.

[Polzin 1996] Polzin, K. L., 1996: Statistics of the Richardson number: Mixing models and finestructure, *J. Phys. Ocean.*, **26**, 1409–1425.

[Polzin 1999] Polzin, K. L., 1999: A rough recipe for the energy balance of quasi-steady internal lee waves, Internal Wave Modeling, Proceedings 'Aha Huliko'a Hawaiian Winter Workshop, P. Müller and D. Henderson, Eds.

[Polzin 2002 a] Polzin, 2002 a: A flux representation of internal wave spectral transports. *J. Phys. Oceanogr.*, submitted.

[Polzin 2002 b] Polzin 2002 b: Idealized solutions for the energy balance of the finescale internal wave field. *J. Phys. Oceanogr.*, submitted.

[Polzin 2002 c] Polzin 2002 c: A rough recipe for the energy balance of the internal tide. *to be sbmitted to J. Phys. Oceanogr.*.

[Polzin et al. 1995] Polzin, K. L., J. M. Toole and R. W. Schmitt, 1995: Finescale parameterizations of turbulent dissipation, *J. Phys. Ocean.*, **25**, 306–328.

[Polzin et al. 1997] Polzin, J. M. Toole, J. R. Ledwell, and R. W. Schmitt, 1997: Spatial variability of turbulent mixing in the abyssal ocean. *Science*, **276**, 93–96.

[Polzin and Firing 1997] Polzin, K. L. and E. Firing, 1997: Estimates of diapycnal mixing using LADCP and CTD data from I8S, WOCE International Newsletter, 29, 39-42.

[Rhines 1970] Rhines, P., 1970: Edge-, bottom- and Rossby waves in a rotating, stratified fluid. *Geophys. Fluid Dyn.*, **1**, 273-302.

[Schmitt et al. 1988] Schmitt, R. W., J. M. Toole, R. L. Koehler, E. C. Mellinger, and K. W. Doherty, 1988: The development of a fine- and microstructure profiler, *J. Atmos. Oceanic Tech.*, **5**, 484–500.

[Wunsch 1998] Wunsch, C. W., 1998: The work done by the wind on the oceanic general circulation. *J. of Phys. Oceanogr.*, **28**, 2332-2342.

[Andrews and McIntyre 1978] Andrews, D. G., and M. E. McIntyre, 1978: On wave action and its relatives. *J. Fluid. Mech.*, **89(4)**, 647-664.

[Andrews et al. 1987] Andrews, D. G., J. R. Holton and C.B. Leovy, 1987: *Middle Atmosphere Dynamics*, Academic Press, Orlando, pp 1-489.

[Charney 1971] Charney, J. G., 1971: Geostrophic turbulence. *J. Atmos. Sci.*, **28**, 1087–1095.

[Charney and Drazin 1961] Charney, J.G., and P.G. Drazin, 1961: Propagation of planetary scale disturbances from the lower into the upper atmosphere. *J. Geophys. Res.*, **66**, 83-109.

[Eliassen and Palm 1961] Eliassen, A. and E. Palm, 1961: On the transfer of energy in stationary mountain waves. *Geophys. Publ., Oslo* **22**, 1-23.

[Gent et al. 1995] Gent, P.R., J. Willebrand, T. McDougall and J.C. McWilliams, 1995: Parameterizing eddy induced transports in ocean circulation models. *J. Phys. Oceanogr.*, **25**, 463-474.

[Ledwell et al. 1998] Ledwell, J. R., A. J. Watson, and C. S. Law, 1998: Mixing of a tracer in the pycnocline, *J. Geophys. Res.*, **103**, 21499–21529.

[Polzin et al. 1996] Polzin, K. L., N. S. Oakey, J. M. Toole and R. W. Schmitt, 1996: Fine- and microstructure characteristics across the northwest Atlantic Subtropical Front. *J. Geophys. Res.*, **101**,

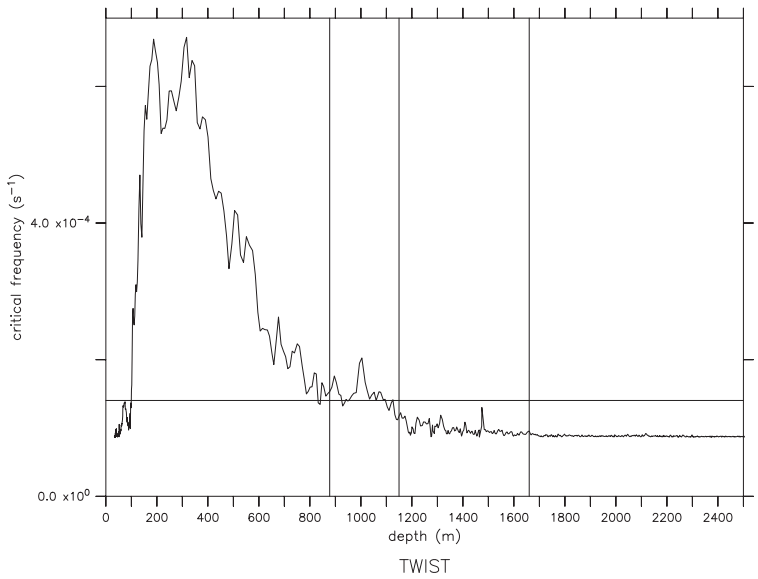

FIG. A3. Estimate of topographic slope derived from the previous figure, expressed in terms of internal wave critical frequency. *Redo as* $N/f\,\tan(\alpha)$ *and use deeper N profile.*

14,111-14,121.

[Polzin et al. 2003] Polzin, K. L., E. Kunze, J. M. Toole, and R. W. Schmitt, 2003. The partition of fine-scale energy into internal waves and subinertial motions. *Journal of Physical Oceanography*, **33**, 234–248.

[Polzin et al. 2004a] Polzin, K. L., 2004a: A heuristic description of internal wave dynamics. *J. Phys. Oceanogr., accepted*.

[Rhines 1979] Rhines, P. B., 1979: Geostrophic Turbulence. *Ann. Rev. Fluid Mech.*, **11**, 401-441.

[Ruddick 1987] Ruddick, B.R. 1987: Anticyclonic Lenses in Large-Scale Strain and Shear. *J. Phys. Oceanogr.*, **17**, 741-750.

[Ruddick and Joyce 1979] Ruddick, B.R. and T.M. Joyce, 1979: Observations of interaction between the internal wavefield and low-frequency flows in the North Atlantic, *J. Phys. Oceanogr.*, **9**, 498-517.

[Tandon and Garrett 1996] Tandon, A., and C. Garrett, 1996: On a Recent Parameterization of Mesoscale Eddies. *J. Phys. Oceanogr.*, **26**, 406-416.

[Tung and Welch 2001] Tung, K. K. and W. Welch, 2001: Remarks on Charney's Note on Geostrophic Turbulence. *J. Atmos. Sci.*, **58**, 2009-2012.

Draft: October 24, 2005